UCLA
UCLA Previously Published Works

Title

EED is required for mouse primordial germ cell differentiation in the embryonic gonad

Permalink

https://escholarship.org/uc/item/22r3s76f

Journal

Developmental Cell, 57(12)

ISSN

1534-5807

Authors

Lowe, Matthew G
Yen, Ming-Ren
Hsu, Fei-Man
et al.

Publication Date

2022-06-01

DOI

10.1016/j.devcel.2022.05.012

Copyright Information

This work is made available under the terms of a Creative Commons Attribution-NonCommercial-NoDerivatives License, available at https://creativecommons.org/licenses/by-nc-nd/4.0/

Peer reviewed

eScholarship.org Powered by the California Digital Library
University of California

Author Manuscript

Author Manuscript

Author Manuscript

Author Manuscript

HHS Public Access

Author manuscript

Dev Cell. Author manuscript; available in PMC 2023 June 20.

Published in final edited form as:

Dev Cell. 2022 June 20; 57(12): 1482–1495.e5. doi:10.1016/j.devcel.2022.05.012.

EED is required for Mouse Primordial Germ Cell Differentiation in the Embryonic Gonad

Matthew G. Lowe[1,2,3,7], **Ming-Ren Yen**[4,7], **Fei-man Hsu**[1,3], **Linzi Hosohama**[1], **Zhongxun Hu**[1], **Tsotne Chitiashvili**[1,2,5], **Timothy Hunt**[1], **Isaac Gorgy**[1], **Matthew Bernard**[1,2], **Sissy Wamaitha**[1], **Pao-Yang Chen**[4,8], **Amander T. Clark**[1,2,3,6,8,9,*]

[1]Department of Molecular Cell and Developmental Biology, University of California, Los Angeles, California, 90095, USA

[2]Molecular Biology Institute, University of California, Los Angeles, California, 90095, USA

[3]Eli and Edythe Broad Center of Regenerative Medicine and Stem Cell Research, University of California, Los Angeles, California, 90095 USA

[4]Institute of Plant and Microbial Biology, Academia Sinica, Taipei City, 11529, Taiwan

[5]Department of Biological Chemistry, University of California, Los Angeles, California, 90095, USA

[6]Jonsson Comprehensive Cancer Center, University of California, Los Angeles, California, 90095 USA

[7]These authors contributed equally

[8]Senior author

[9]Lead Contact

Summary

Development of primordial germ cells (PGCs) is required for reproduction. During PGC development in mammals, major epigenetic remodeling occurs which is hypothesized to establish an epigenetic landscape for sex-specific germ cell differentiation and gametogenesis. In order to address the role of Embryonic Ectoderm Development (EED) and Histone 3 lysine 27 trimethylation (H3K27me3) in this process, we created an EED conditional knockout mouse and show that EED is essential for regulating the timing of sex-specific PGC differentiation in

*Correspondence: clarka@ucla.edu.

Author Contributions

M.G.L. designed and performed all experiments, maintained the mouse lines and wrote the manuscript. Z.H. and I.G. designed and performed the experiments. T.C. performed the X/A expression analysis. M.B. and S.W performed the co-IP. L.H. established the mouse lines. T.H. maintained the mouse lines. M.R.Y. and P.Y.C. performed bulk RNA-seq and ChIP-seq analysis. F.M.H. performed the transposon, whole genome bisulfite and single cell RNA sequencing analysis. A.T.C. designed and oversaw all experiments, wrote the manuscript, maintained all university compliances and attained funding for the experiments.

Publisher's Disclaimer: This is a PDF file of an unedited manuscript that has been accepted for publication. As a service to our customers we are providing this early version of the manuscript. The manuscript will undergo copyediting, typesetting, and review of the resulting proof before it is published in its final form. Please note that during the production process errors may be discovered which could affect the content, and all legal disclaimers that apply to the journal pertain.

Declaration of Interests

The authors declare no competing interest.

Author Manuscript Author Manuscript Author Manuscript Author Manuscript

both ovaries and testes, as well as X chromosome dosage decompensation in testes. Integrating chromatin and whole genome bisulfite sequencing of epiblast and PGCs, we identified a poised repressive signature of H3K27me3/DNA methylation which we propose is established in the epiblast where EED and DNMT1 interact. Thus, EED joins DNMT1 in regulating the timing of sex-specific PGC differentiation during the critical window when the gonadal niche cells specialize into an ovary or testis.

Graphical Abstract

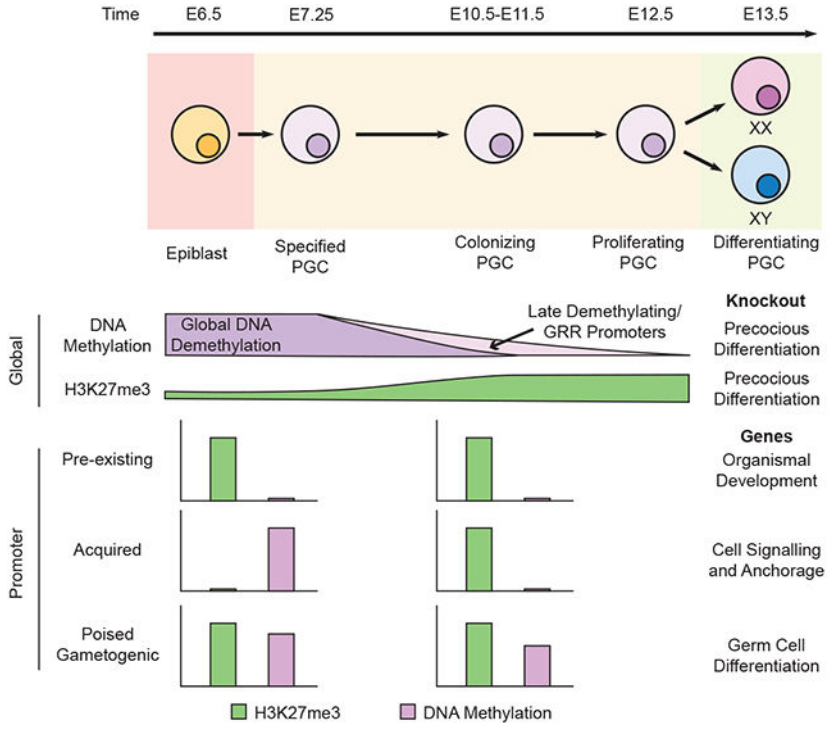

eTOC

Lowe and Yen et al. show that promoters of germ cell differentiation genes in the mouse post-implantation epiblast are enriched in H3K27me3 and DNA methylation, with EED regulating the timing of primordial germ cell (PGC) differentiation. This expands our understanding of the epigenetic regulation of PGC differentiation in the embryonic gonad.

Introduction

Primordial germ cells (PGCs) are the embryonic progenitors of the germline and their correct epigenetic regulation and sex-specific differentiation is essential for establishing fertility in the adult. In the mouse embryo, the PGC stage of germline development takes around seven days beginning at embryonic day (E) 6.25 with specification of PGCs from the epiblast and ending at E13.5, after the committed PGCs have colonized the embryonic gonad (Ginsburg et al., 1990; Saitou and Yamaji, 2012). In the last 24 hours of PGC development, between E12.5-E13.5, XX and XY PGCs heterogeneously initiate sex-specific differentiation in response to gonadal cues (Jameson et al., 2012). This differentiation is

Author Manuscript Author Manuscript Author Manuscript Author Manuscript

accompanied by locus-specific epigenetic changes to promoters and enhancers combined with global remodeling of chromatin (Guibert et al., 2012; Hackett et al., 2013; Hajkova et al., 2002; Hill et al., 2018; Kobayashi et al., 2013; Liu et al., 2014; Seisenberger et al., 2012; Yokobayashi et al., 2013; Zheng et al., 2016). Following sex-specific differentiation the germ cells enter cell cycle arrest by E15.5, either in prophase I of meiosis I as XX PGCs become meiotic germ cells, or in G0 cell cycle arrest XY PGCs become pro-spermatogonia (Baltus et al., 2006; Western et al., 2008). It is hypothesized that epigenetic remodeling during the final stages of PGC development is necessary to generate an epigenome conducive to sex-specific differentiation and high-fidelity gametogenesis (Hajkova et al., 2002).

The epigenetic mark trimethylation of lysine 27 on histone 3 (H3K27me3) has long been known to enrich in PGC nuclei following specification from the epiblast (Seki et al., 2005), however little is known about its role in PGC biology. H3K27me3 is generated by polycomb repressor complex 2 (PRC2), composed of the core components Enhancer of Zeste 2 (EZH2), Embryonic Ectoderm Development (EED) and Suppressor of Zeste 12 (SUZ12) (Kuzmichev et al., 2002; Schuettengruber et al., 2017). High levels of EED and SUZ12 are detected in PGC nuclei, concurrent with a global enrichment of H3K27me3 in XY and XX PGCs during development (Mallol et al., 2019; Napoles et al., 2007; Seki et al., 2005). In contrast, while H3K27me3 is initially enriched on the inactive X (Xi) chromosome of XX PGCs at the time of specification, the Xi is rapidly depleted of PRC2 components and H3K27me3 between E8.5 - E9.5 just prior to X chromosome reactivation and repression of the long non-coding RNA X-inactive specific transcript (*Xist*) (Lopes et al., 2008; Mallol et al., 2019; Napoles et al., 2007; Seki et al., 2005; Sugimoto and Abe, 2007). Recent studies have revealed that both the nuclear increase in H3K27me3, and the loss of H3K27me3 from the Xi are dependent upon the transcription factor Prdm14 (Mallol et al., 2019). After the PGCs have settled into the gonad, H3K27me3 redistributes transiently to the nuclear periphery where it is visualized as a bright ring from E11.5 until the end of PGC sex-specific differentiation (Prokopuk et al., 2017). Nuclear enrichment of H3K27me3 by E9.5 is concurrent with genome wide depletion of DNA methylation, except in locus-specific patches where both H3K27me3 and DNA methylation are identified at CG-island (CGI)-containing promoters of germ cell differentiation genes called "*late demethylators*" (Kobayashi et al., 2013; Seisenberger et al., 2012) or "*germline reprogramming responsive genes*" (GRRs) (Hill et al., 2018) which regulate the timing of PGC differentiation in the embryonic gonad (Hargan-Calvopina et al., 2016) as well as certain transposable elements (TEs) (Liu et al., 2014).

To evaluate locus-specific sites of H3K27me3 enrichment in PGCs at the time of gonadal colonization, chromatin immunoprecipitation (ChIP) followed by sequencing of PGCs isolated at E11.5, E12.5 and E13.5 have revealed that H3K27me3 is enriched at the promoters of genes involved in embryonic and germ cell development, as well as some classes of transposons (Lesch et al., 2013; Liu et al., 2014; Ng et al., 2013; Sachs et al., 2013; Yokobayashi et al., 2013). This promoter enrichment is consistent with other histone modifications that are predicted to synergize with H3K27me3 in PGCs, both in regulating the timing of PGC differentiation as well as maintaining genomic integrity. For example, monoubiquitination at lysine 119 of histone H2A (H2AK119ub1) generated by

Author Manuscript Author Manuscript Author Manuscript Author Manuscript

polycomb repressor complex 1 (PRC1)/RNF2 has been shown to regulate the timing of XX PGC differentiation and entrance into meiosis through regulation of the *Stra8* promoter (Yokobayashi et al., 2013). Addtionally, H3K9me3/SETDB1 and H4R3me2/PRMT5 have broad roles regulating TE repression in PGCs (Kim et al., 2014; Liu et al., 2014) with H3K9me3 enrichment at some TEs coinciding with both H3K27me3 and DNA methylation (Liu et al., 2014). Repression of TEs throughout germline development is critical because some TEs are still capable of active transposition in mice (Dewannieux et al., 2004; Richardson et al., 2017). Taken together, these studies suggest that H3K27me3 may function in concert with other epigenetic marks to regulate PGC development. However, chemical inhibition of EZH1/2 for 72-hours in *ex vivo* E11.5 gonadal organ culture (Prokopuk et al., 2017, 2018) as well as a hypomorphic mutation in *Eed* (Stringer et al., 2018) had no observable effect on the PGCs despite depletion of H3K27me3.

Given the dynamic nature of H3K27me3 during the course of PGC development *in vivo*, we evaluated the role of EED in PGCs by performing a conditional deletion of EED at the time of PGC specification using Blimp1-Cre (BC). EED is required to add and retain H3K27me3 at nucleosomes, therefore a null deletion in EED causes loss of H3K27me3 from chromatin (Yu et al., 2009). Our work shows that deleting EED and removing H3K27me3 from PGC chromatin regulates the timing of PGC differentiation between E11.5-E13.5, placing H3K27me3 in a synergistic pathway with DNA methylation and H2AK119ub1 in regulating the response of PGCs to the niche during sex-determination. Moreover, we identify a distinct subset of germline promoters within the epiblast uniquely marked with both H3K27me3 and DNA methylation at the time of PGC specification. Finally, our data also reveals that H3K27me3/EED regulates decompensation of X-linked genes in XY PGCs at the end of PGC development (Sangrithi et al., 2017), providing new insights into the phenomenon of X chromosome dosage decompensation in the XY prenatal germline.

Results

Loss of EED Leads to Reduced PGC Number Within the Gonads

To evaluate the role of EED/H3K27me3 in PGCs, we crossed the $Eed^{fl/fl}$ (Yu et al., 2009) allele with *Blimp1-Cre* (BC) (Ohinata et al., 2005), to create an EED conditional knockout embryo (ECKO). The *BC* mouse was chosen as *Blimp1 is* expressed in the PGC precursors within the epiblast of mouse embryos, and continues to be expressed in PGCs until soon after gonadal colonization (Ohinata et al., 2005) (Figure 1A). In addition, we also crossed the $Eed^{fl/fl}$ mice with *Oct4*-GFP (OG) (Lengner et al., 2007) to create a GFP reporter to isolate GFP+ PGCs by fluorescence activated cell sorting (FACS). Using this tool, we performed FACS to isolate *Oct4*-GFP+ PGCs from genital ridges at E10.5 and E11.5 (colonizing PGCs) as well as from the embryonic gonads of XX and XY embryos at E12.5 and E13.5 when H3K27me3 levels are at their highest (Figure 1A and S1A). Using this approach, we discovered a significant reduction in ECKO PGC number compared to controls starting at E11.5 in XX and E12.5 in XY embryos (Figure 1B). Linear regression analysis of PGC number over time shows a distinct difference in doubling time between control and ECKO PGCs, with the effect on XX ECKO PGCs being particularly pronounced (Figure 1C). To evaluate the localization of PGCs within the embryonic gonad at E13.5, we

Author Manuscript Author Manuscript Author Manuscript Author Manuscript

performed immunofluorescence (IF) of embryonic testes and ovaries and show that VASA+ XY ECKO PGCs correctly localize to the AMH+ testis cords (Figure S1B) while XX ECKO PGCs tend to localize into small clusters or nests (Figure S1C). This result indicates that EED regulates the size of the PGC progenitor pool within the gonad between E11.5-E13.5, and does not have an obvious effect on PGC numbers prior to gonadal colonization.

Given the dramatic reduction in PGC number, we next evaluated the presence or absence of H3K27me3 in ECKO and control PGCs at E11.5 and E13.5 using IF. Using the germline transcription factor TFAP2C to mark PGCs (Weber et al, 2010), we show that by E11.5 the vast majority of TFAP2C+ PGCs in ECKO embryos no longer have detectable H3K27me3 (Figure S1D-E). Notably, while the majority of ECKO PGCs do localize properly to the developing gonad, we did observe some rare TFAP2C+ cells still outside the XX embryonic gonad at E11.5 (Figure S1F), which might suggest some developmental delay/mislocalization of ECKO PGCs. However, by E13.5, no VASA+ PGCs were identified outside the embryonic gonad and ECKO PGCs were almost completely depleted of H3K27me3 (Figure 1D-E). Taken together, deleting EED in PGCs leads to loss of H3K27me3 from PGC chromatin by E11.5 and this accompanied by a phenotypic reduction in PGC number between E11.5 and E13.5.

To explore the cause of reduced PGCs at E13.5, we performed IF for the apoptotic marker cleaved PARP (cPARP) (Boulares et al., 1999) and found no significant difference in the fraction of apoptotic PGCs in ECKO embryos relative to control (Figure 1F-G). Additionally, we examined Ki67 which marks cycling cells (Gerdes et al., 1983) and found no significant difference between control and ECKO PGCs at E13.5 (Figure S1G-H). However, it is important to note that Ki67 is still expressed in oocytes initiating meiotic arrest (Traut et al., 2002). This suggests that the reduction in PGC number observed in both sexes by E13.5 is not due to increased apoptosis or entrance into G0.

Given that H3K27me3 becomes enriched in PGCs as DNA methylation is reduced (Seki et al., 2007, 2005), we next evaluated whether loss of EED/H3K27me3 is associated with failure to lose DNA methylation from the PGC genome by examining 5mC and 5hmC levels using IF. Staining for 5mC in XY and XX ECKO PGCs at E13.5 revealed that global levels of DNA methylation were still depleted in the absence of EED/H3K27me3 (Figure S2A-B). Likewise, the generation of distinct 5hmC foci were also unaffected by loss of EED/H3K27me3 (Figure S2C-D). Therefore, the loss of EED/H3K27me3 does not prevent the global depletion of DNA methylation. In contrast, the active mark H3K27ac was significantly enriched in E13.5 XY PGCs following loss of EED/H3K27me3 consistent with previous reports (Pasini et al., 2010) (Figure S2E-F). While the E13.5 XX PGCs did not have significantly higher H3K27ac signal, they did show a marginal increase and generally had higher H3K27ac signal than XY PGCs.

EED Regulates Precocious Differentiation in the Testis

In order to evaluate whether a deletion of EED in PGCs effects gene expression and identify a mechanism for the reduced PGC number in both sexes, we performed RNA-Seq in XY GFP+ PGCs isolated by FACS from individual embryos at E11.5 and E13.5. Principle component analysis (PCA) of RNA-seq data revealed a major shift in gene

Author Manuscript Author Manuscript Author Manuscript Author Manuscript

expression (PC1) between E11.5 and E13.5 regardless of genotype (Figure 2A). This is expected, and coincides with gonadal niche sex-determination between E11.5-E13.5 which then instructs the PGCs to adopt a sex-specific fate. Additionally, we observed a distinct separation at E13.5 when comparing ECKO and control PGCs along PC2, which indicates a transcriptional shift on account of EED loss. Although ECKO and control PGCs at E11.5 cluster closer together, a small number of significant differentially expressed genes (DEGs) were identified (Table S1), with the vast majority (89%) being upregulated (Figure 2B and Table S1). In order to identify whether the upregulated genes at E11.5 are direct targets of EED/H3K27me3, we evaluated previously published H3K27me3 ChIP-seq data of E11.5 wild-type PGCs (Sachs et al., 2013), and discovered that 81% of upregulated E11.5 XY DEGs are reported to have promoters enriched for H3K27me3. (Figure 2C and Table S1). Therefore, the majority of differentially upregulated genes in the ECKO PGCs are likely to occur as a direct consequence of H3K27me3 loss. Because H3K27me3 is known to also mark TEs in PGCs (Liu et al., 2014), we next assessed whether loss of EED led to an upregulation of TEs at E11.5 and E13.5. We observe a weak positive correlation between upregulated TE's that are known to be enriched in H3K27me3 (Figure S3A-B), indicating that EED/H3K27me3 does not have a major role in repressing TEs in PGCs.

A recently described phenomenon in the XY germline is X chromosome dosage decompensation, which is initiated at the end of PGC development between E12.5-E14.5 (Sangrithi et al., 2017). Given that *Xist* is not expressed in XY PGCs (McCarrey and Dilworth, 1992), we evaluated whether EED is participating in X chromosome dosage decompensation by examining X chromosome/Autosome (X/A) ratios in XY ECKO and control PGCs (Figure 2D-E). Our data shows that despite there being no significant difference in H3K27me3 promoter abundance between autosomes and the X chromosome in E13.5 XY PGCs (Figure S3C), the X/A ratio in E13.5 ECKO XY PGCs is significantly higher than control (Figure 2D). Using a Hypergeometic test, we discovered that X-linked genes are statistically over-represented amongst the direct targets of EED in XY PGCs at E13.5 (Figure S3D) and that the X-linked genes with known H3K27me3 promoter enrichment appear more sensitive to loss of EED relative to autosomal genes (Figures 2E). Taken together, this data indicates that X chromosome decompensation in the XY germline involves EED/H3K27me3 and that this mode of regulation is likely to be direct.

Similar to E11.5, at E13.5 there is a greater proportion of upregulated genes (59%) in the ECKO PGCs (Figure 2F). Using previously published E13.5 H3K27me3 ChIP-Seq data from FACS isolated PGCs (Liu et al., 2014), we show that approximately half the upregulated DEGs at E13.5 have H3K27me3 promoter enrichment in control PGCs at E13.5; suggesting that depletion of H3K27me3 from chromatin prior to sex-specific differentiation may have indirect or secondary effects on gene expression (Figure 2G and Table S1). Similarly, the vast majority of downregulated DEGs at E11.5 and E13.5 do not contain H3K27me3 and are likely indirect effects of an EED deletion in PGCs (Figures 2C and G). Gene ontology (GO) analysis of the upregulated DEGs at E13.5 revealed an enrichment for genes involved in spermatogenesis and piRNA metabolism (Figure 2H). In contrast, the downregulated DEGs were enriched for GO terms associated with cell cycle and cell division (Figure 2I). Exiting the cell cycle in XY PGCs is a progressive process associated with differentiation into pro-spermatogonia (Western et al., 2008). To

Author Manuscript Author Manuscript Author Manuscript Author Manuscript

confirm that XY PGCs are precociously differentiating downstream of an EED mutation, we performed IF for MILI (PIWIL2) which is expressed in cytoplasmic pi-bodies of pro-spermatogonia (Aravin et al., 2008). Our results show that in the absence of EED, most XY PGCs at E13.5 have MILI in cytoplasmic pi-bodies while only rarely detected in controls (Figure 2J-K). Given the precocious PGC differentiation observed in PGCs at E13.5, combined with the reduction in PGC number at E12.5, we performed single cell RNA sequencing of E12.5 in control and ECKO XY PGCs using Smart-seq to evaluate whether precocious differentiation begins at E12.5 (Figure 2L and S3E). These results show a reduction in *Nanog* levels in about half of the ECKO PGCs indicating preparation for exiting the PGC stage, however *Miwi2 (Piwil4)* was not concomitantly upregulated suggesting that precocious differentiation of XY PGCs into pro-spermatogonia initiates between E12.5 and E13.5. Curiously, we identified de-repression of *Hoxa1* and *Hoxb1* in a small number of cells which are indicative of somatic gene expression. Finally, some rare ECKO XY PGCs also exhibited an increased in *Stra8*, a gene required for meiotic initiation (Baltus et al., 2006). However, this was not a major phenomenon, occurring in only 6/26 ECKO PGCs (Figure S3E). Taken together these results suggest that EED is necessary to prevent precocious differentiation of XY PGCs into pro-spermatogonia following sex specific differentiation of the gonadal niche, and that EED participates in the XY PGC X chromosome dosage decompensation at E13.5.

EED Regulates Precocious Differentiation in the Ovary

Given that XX PGC numbers were reduced in the ovaries of ECKO embryos, we next turned to the hypothesis that similar to RNF2/PRC1 (Yokobayashi et al., 2013), EED/PRC2 regulates XX PGC differentiation timing. Following deletion of *Rnf2*, the meiotic initiator *Stra8*, is precociously upregulated driving entrance of XX PGCs into meiosis (Yokobayashi et al., 2013). To evaluate whether EED/PRC2 functions upstream of PRC1 in PGCs, we performed IF for the PRC1 deposited epigenetic mark monoubiquitin of lysine 119 on histone 2A (H2AK119ub1) (de Napoles et al., 2004) at E13.5 (Figure S4A-B). Through this, we show that global H2AK119ub1 enrichment is not altered in XX and XY PGCs despite the absence of EED/HK27me3.

In order to evaluate how loss of EED may affect X chromosome dosage compensation in XX PGCs, we performed RNA sequencing of FACS isolated OG+ PGCs from XX ECKO and control embryonic ovaries at E11.5. This data showed that deletion of EED had no effect on PGC X-chromosome dosage compensation (Figure 3A) and only weak effects on TE expression at E11.5 (Figure S3F). Analysis of autosomal genes revealed a relatively small number of DEGs at E11.5, the majority which were upregulated (81%) (Figure 3B and Table S1). In particular, *Stra8* was upregulated and genes associated with proliferative PGCs (*Pecam1 and Klf5*) were downregulated (Figure 3C-D) (Saitou and Yamaji, 2012). Similar to XY PGCs (Figure 2), analysis of H3K27me3 ChIP-Seq data sets (Sachs et al., 2013) revealed that the majority of upregulated DEGs (78%) at E11.5 were known to have promoter enrichment of H3K27me3, and thus are likely direct targets of EED (Figure 3E and Table S1). Given that after E11.5 H3K27me3 levels are reduced at the *Stra8* locus in wild type XX PGCs (Figure 3F) and the key role that *Stra8* plays in regulating XX PGC

Author Manuscript Author Manuscript Author Manuscript Author Manuscript

entrance into meiosis, this suggests a potential role for H3K27me3 in regulating meiotic initiation.

In order to evaluate PGC identity in ECKO and control PGCs at E12.5, we performed single cell RNA-seq using Smart-seq (Figure 3G and S4C-D). This result confirms that *Stra8* de-repression has begun by E12.5 in all ECKO XX PGCs with heterogenous upregulation of the meiotic marker Synaptonemal Complex Protein 3 *Sycp3* and *Meioc* which marks prophase I meiosis I arrested PGCs (Soh et al., 2017). Furthermore, the down regulation of *Nanog* and *Tfap2c* indicates exit from mitosis and entrance into meiosis. Intriguingly, like XY PGCs, we also observed upregulation of the somatic patterning genes *Hoxa1* and *Hoxb1* in some ECKO meiotic PGCs (Figure S4C). Through a comparison with recently published 10x single cell sequencing of PGCs (Zhao et al., 2020) we found that control E12.5 PGCs in our data set correlated with E12.5 PGCs from (Zhao et al., 2020) (Figure S4D). In contrast, the E12.5 ECKO PGCs showed a stronger correlation to E14.5 PGCs consistent with precocious differentiation (Figure S4D).

Finally, to confirm that XX PGCs are precociously entering into meiosis, we used IF to evaluate the meiotic marker SYCP3, and show that the majority of ECKO PGCs at E13.5 are SYCP3+ (Figure 3H-I). In summary, the reduction in PGC number in XX and XY embryos between E11.5 and E13.5 is due to precocious differentiation of PGCs which involves exit from the mitotic cell cycle and formation of meiotic oocytes or pro-spermatogonia respectively.

Some Gametogenesis Genes are Co-Enriched for H3K27me3 and DNA Methylation in the Epiblast

Given that H3K27me3 in PGCs could be inherited from the epiblast cells at the time of PGC specification as well as through enrichment in PGC chromatin after specification, we next compared H3K27me3 promoter abundance in the epiblast at E6.5 (Yang et al., 2018) to PGCs at E11.5 (Sachs et al., 2013). Using a ≥2-fold cut-off, we identified 3,783 promoters with H3K27me3 enrichment in both E6.5 epiblasts and E11.5 PGCs, referring to these promoters as "*pre-existing*" under the assumption that H3K27me3 in the E6.5 epiblast was likely maintained following PGC specification (Figure 4A and S5A-B). Additionally, we identified 2,852 promoters in PGCs that were significantly enriched with H3K27me3 at E11.5, but not at E6.5, which we call "*acquired*" with the assumption that H3K27me3 is acquired at these sites during PGC differentiation.

Given that EED regulates the timing of PGC differentiation similar to DNMT1, we next explored a potential relationship between H3K27me3 and DNA methylation in the context of the pre-existing or acquired promoter categories. Using whole genome bisulfite sequencing (WGBS) data sets from E6.5 epiblast and E11.5 PGCs (Seisenberger et al., 2012), we examined average DNA methylation levels in the pre-existing and acquired H3K27me3 promoter categories (Figure 4B). Because PRC2 recognizes unmethylated CpG rich sequences (Heeringen et al., 2014; Mendenhall et al., 2010) and DNA methylation and H3K27me3 tend to be mutually exclusive (Bartke et al., 2010; King et al., 2016; Li et al., 2018), we hypothesized that promoters in the epiblast containing pre-existing H3K27me3 should in general also be hypomethylated and indeed this is the case (Figure 4C). In

Author Manuscript Author Manuscript Author Manuscript Author Manuscript

contrast, promoters that acquired H3K27me3 in PGCs were hypermethylated in the E6.5 epiblast and became hypomethylated at E11.5 in PGCs. This is consistent with previously published work showing that loss of DNA methylation can cause spreading of H3K27me3 (van Mierlo et al., 2019; Murphy et al., 2013). Evaluating CpG content of these promoters based on the criteria of (Mohn et al., 2008), revealed that the majority of pre-existing H3K27me3 promoters are categorized as high and intermediate CpG content (HCP, ICP) whereas promoters that acquired H3K27me3 in PGCs corresponded to low (LCP) and ICP (Figure 4D). This fits well with previous work showing that high CpG content is typically associated with low levels of DNA methylation and high levels of H3K27me3 (Chen et al., 2018; Mendenhall et al., 2010). Taken together, this analysis reveals that the retention and acquisition of promoter H3K27me3 is inversely correlated with DNA methylation as PGCs differentiate.

Given that the late demethylators and GRRs contain significant DNA methylation at E6.5 despite being categorized as ICP and HCP (Hill et al., 2018; Seisenberger et al., 2012) we predicted that they might acquire H3K27me3 following PGC specification. To address this, we evaluated the late demethylating promoters identified by (Seisenberger et al., 2012), 45% of which exhibit H3K27me3 promoter methylation in E11.5 PGCs (Sachs et al., 2013) (Figure S5C). Categorizing these promoters with H3K27me3 revealed that while some are acquired as predicted, a greater proportion (60%) had pre-existing H3K27me3. Repeating this analysis for the GRR promoters identified by (Hill et al., 2018), we also found that (60%) were marked by H3K27me3, and the vast majority of the marked promoters (80%) were pre-existing (Figure S5D). We next examined the extent that late demethylating promoters are enriched for H3K27me3 via scatterplot (Figures S5E) and observed a similar pattern to what was seen in all promoters (Figure S5A). GO analysis of the late demethylating promoters containing H3K27me3 at E11.5 identified categories of genes involved in meiotic cell cycle, spermatogenesis and piRNA metabolic process (Figure 4E). Critically, these are the same GO groups regulated by DNMT1 in PGCs (Hargan-Calvopina et al., 2016) suggesting a potential connection between H3K27me3 and DNA methylation in regulating PGC development.

Given that PGCs lose DNA methylation after specification from the epiblast, we predicted that the relationship between DNA methylation and H3K27me3 likely begins in the epiblast. Evaluating methylation levels of the late demethylating promoters at E6.5 (Seisenberger et al., 2012) revealed that pre-existing promoters of late demethylating genes also begin with high levels of DNA methylation in the epiblast (Figure 4F, S5E-F). This subgroup of pre-existing H3K27me3 promoters that are also enriched in DNA methylation includes critical germline genes such as *Stra8* and *Dazl* (Figure S5E). Analyzing the CpG content of late demethylating promoters with pre-existing H3K27me3 and high levels of DNA methylation (Figure 4F and S5F, red box) mostly correspond to promoters with ICP and HCP (Figure 4G). Taken together, these results suggest a potential functional relationship between EED/H3K27me3 and DNMT1 in PGC development.

Author Manuscript Author Manuscript Author Manuscript Author Manuscript

Gametogenesis Genes are Coregulated by EED and DNMT1

In order to characterize a potential relationship between EED and DNMT1, we re-analyzed the DNMT1 PGC conditional knockout (DCKO) bulk RNA-seq data set at E13.5 (Hargan-Calvopina et al., 2016) and discovered that 69% of the upregulated DEGs in the E13.5 XY DCKO PGCs have promoters enriched in H3K27me3 (Liu et al., 2014) (Figure 5A and table S1). We then compared the overlapping upregulated DEGs between the E13.5 XY DCKO and ECKO PGC after filtering out genes which are only expressed in both data sets and discovered that 60% of DCKO upregulated genes at E13.5 are also upregulated in ECKO XY PGCs (Figure 5B-C and S6A). This overlapping set of DEGs are significantly enriched for GO terms involved in gametogenesis (Figure 5D) and the CpG content of their promoters is mostly ICP and HCP (Figure 5E).

Given the overlap, we next asked whether EED/H3K27me3 is required to maintain DNA methylation at these promoters. To achieve this, we performed WGBS of control and ECKO GFP+ PGCs isolated from embryos at E10.5 and E11.5 using FACS (Figure S6B). E10.5 and E11.5 were chosen because this is the time when late demethylators still have observable levels of DNA methylation, whereas at E13.5 late demethylators have fully demethylated. This result shows that loss of EED in PGCs is accompanied by a reduction in global levels of DNA methylation at E10.5 (Figure 5F). However, at a promoter level, we did not observe a significant difference in DNA methylation between control and ECKO PGCs at E11.5 in selected late demethylating, overlapping DEG promoters (Figure 5G and S6C). Therefore, our data suggest that DNA methylation at late-demethylating promoters in PGCs is not dependent upon EED.

To examine a potential relationship between EED and DNMT1 in the epiblast, we performed native co-immunoprecipitation (co-IP) to evaluate the endogenous interaction between EED and DNMT1. For this experiment we used Epiblast Like cells (EpiL5/20/2022 4:38:00 PMCs) which are equivalent to the epiblast of post-implantation embryos competent for PGC specification (Hayashi et al., 2011), and mouse embryonic stem cells (ESCs) cultured in serum +LIF (Figures 5H-I and S6D). Our results show when using EED for IP (Figure 5H-I) DNMT1 and EED interact. Additionally, we also detect EZH2 and DNMT1s binding partner UHRF1 in the EED IP pulldowns with no detectable signal in the IgG negative control. EED is known to have multiple isoforms (Bracken et al., 2006; Liu et al., 2019; Montgomery et al., 2007) and regardless of whether EpiLC or ESCs were used, we selectively enriched for a shorter isoform (~45 kDa) when blotting for EED in the IP experiments with the EED antibody. Interestingly, when performing the reciprocal pull down with DNMT1 antibody in serum +LIF ESCs, we also selectively pull down the shorter EED isoform alongside UHRF1 (Figure S6D). Taken together we identified a unique subset of gametogenesis genes which are enriched for both H3K27me3 and DNA methylation in the E6.5 epiblast prior to PGC specification, where we also see an interaction between EED and DNMT1. From this result, we propose a model by which this epigenetic signature is established in the epiblast and maintained throughout PGC development to regulate PGC differentiation timing (Figure 6).

Author Manuscript Author Manuscript Author Manuscript Author Manuscript

Discussion

In this study, we show that EED is essential to regulate the timing of PGC differentiation between E11.5-E13.5, and X chromosome dosage decompensation in XY PGCs at E13.5. Through this, we identified a functional role for EED in PGC development before E13.5. Additionally, we show a relationship between DNMT1/DNA methylation and EED/H3K27me3 that begins prior to PGC specification in the epiblast to regulate repression of gametogenesis genes. Collectively, our data further clarifies the epigenetic landscape that regulates PGC differentiation and identifies a new mechanism for regulating X chromosome decompensation in XY germ cells at E13.5.

One of the major findings in the current study is the direct role for EED in X chromosome decompensation in E13.5 XY PGCs. X chromosome compensation in XX cells is regulated by the long noncoding RNA *Xist* as well as H3K27me3, which becomes dynamically re-distributed during the process of X-chromosome reactivation in XX PGCs. During X reactivation, H3K27me3 is simultaneously removed from the Xi chromosome in XX PGCs, while becoming globally enriched in the nucleus of PGCs in both sexes between E8.5-E9.5 (Mallol et al., 2019; Napoles et al., 2007; Seki et al., 2005). Here, we show that loss of EED in XX PGCs does not lead to an increase in the X/A ratio at E11.5, indicating that loss of EED does not have a major impact on X-linked gene expression in XX PGCs prior to sex-determination. Instead, we found that EED had a role in X chromosome decompensation during the transition of XY PGCs to pro-spermatogonia, with X-linked genes in XY PGCs being significantly more sensitive to loss of EED at E13.5 than H3K27me3 marked genes on autosomes. Future studies aimed at the role of X chromosome decompensation in regulating the biology of pro-spermatogonia, establishment of long-term self-renewing spermatogonia and spermatogenesis are warranted.

Despite the well-known complex dynamics of H3K27me3 global enrichment during PGC development (Figure 1A), chemical inhibition of EZH1/2 using *ex vivo* embryonic gonadal organ cultures suggested that EZH1/2 does not regulate PGC number (Prokopuk et al., 2017, 2018). This was confirmed by a recent manuscript involving an EZH2 conditional knockout which showed no loss of PGCs before E13.5, and instead a reduction in PGC number, together with TE de-repression from E16.5 (Huang et al., 2021). A direct comparison of EED and EZH2 null mutant phenotypes in mouse intestinal villus cells revealed that a EZH2 null phenotype is less severe than the EED null phenotype (Jadhav et al., 2020). This supports the finding that a more severe phenotype is to be anticipated when deleting EED compared to EZH2, which in our study involved the emergence of a PGC phenotype between E11.5-E12.5 in the EED null mutant embryos.

Conditional deletion of *Dnmt1* in PGCs leads to a substantial increase in *Stra8* RNA by E13.5 and precocious entry into meiosis (Hargan-Calvopina et al., 2016). Conversely, deletion of Ten eleven translocation 1 (*Tet1*) which oxidizes 5mC to 5hmC results in delayed entrance into meiosis (Yamaguchi et al., 2013). Given that *Stra8* was not significantly induced in *Dnmt1* conditional knockout PGCs at E11.5, this result implies that other facultative repressors shield *Stra8* from precocious expression until E11.5. One of these repressors was previously identified as PRC1/RNF2 which represses *Stra8* in XX PGCs at

Author Manuscript Author Manuscript Author Manuscript Author Manuscript

E11.5 (Yokobayashi et al., 2013). Here, we show that EED (a binding partner of PRC1 proteins) is also necessary to repress *Stra8* in XX PGCs at E11.5. Intriguingly, a conditional deletion of Eed (this study) and *Ezh2* (Huang et al., 2021) in PGCs has no effect on the global levels of H2AK119ub1 in PGC nuclei. Similarly, loss of Rnf2 does not affect the global levels pf H3K27me3 (Yokobayashi et al., 2013). This indicates that while the global enrichment of H3K27me3 and H2AK119ub1 in PGC nuclei are not dependent upon one another, they appear to localize at certain promoters to co-regulate key loci such as *Stra8*. Given that EED and DNMT1 both act at the *Stra8* promoter, we asked whether EED is functionally required to maintain DNA methylation at the gametogenesis late-demethylating promoters in PGCs. Our data shows that EED is not required to maintain DNA methylation at the late demethylating promoters, suggesting that DNMT1 may utilize other chromatin binding partners or chromatin signatures to maintain DNA methylation at gametogenesis genes following PGC specification. Taken together, our data indicates that at least three repressive epigenetic modifications converge on the *Stra8* promoter to regulate expression timing in PGCs (DNMT1/DNA methylation, EED/H3K27me3 and RNF2/H2AK119ub1).

Although EED is not required to maintain DNA methylation at gametogenesis promoters in PGCs, future studies could evaluate whether DNA methylation is involved in maintenance of EED/H3K27me3 at gametogenesis promoters in PGCs. UHRF1 protein is repressed in PGCs, therefore maintenance DNA methylation is not thought to be the mechanism by which DNMT1 functions in PGCs. Recent work has shown that DNMT1 has *de novo* methyltransferase activity when targeted to regions with densely methylated CGs maintaining DNA methylation in a “neighborhood” dependent manner (Haggerty et al., 2021; Wang et al., 2020). There are two major forms of DNA methylation at gametogenesis promoters in PGCs, 5-methylcytosine (5mC) and 5-hydroxymethyl cytosine (5hmC) (Hackett et al., 2013). TET1, the enzyme that oxidizes 5mC to 5hmC is known to recruit PRC2 to high CpG content regions (Wu et al., 2011). Therefore, it is tempting to speculate that the presence of 5hmC at gametogenesis promoters in PGCs enables the enrichment of H3K27me3 at these sites through PRC2.

Our data shows that the co-enrichment of DNA methylation and H3K27me3 at gametogenesis promoters begins in the epiblast, before PGC specification. To address the relationship between EED and DNMT1 in pluripotent cells prior to PGC specification we used native co-IP in ESCs and EpiLCs to show that EED and DNMT1 interact, providing a potential mechanism for the coordinated activity of EED and DNMT1 in the epiblast. A caveat to these studies is that the native IP interaction is weak. This could mean that DNMT1 and EED interact in only a small fraction of protein complexes, or that this interaction is indirect. In addition, a second unexpected finding was that the shorter isoform of EED was preferentially pulled down in the Co-IPs using the EED and the DNMT1 antibody. Different isoforms of EED have previously been described (Bracken et al., 2006; Cao et al., 2014; Liu et al., 2019) and are known to incorporate into a functional PRC2 complex (Montgomery et al., 2007). However, the relevance of the shorter isoform in the putative EED/DNMT1 interaction is not known. In ESCs repression of gametogenesis genes is regulated by PCGF6, a component of the PRC1.6 complex (Endoh et al., 2017; Zhao et al., 2017). In this cellular context, PCGF6 recruits the histone modifying enzymes G9A/GLP to deposit H3K9me2 at gametogenesis promoters (Liu et al., 2020). PRC2 components

Author Manuscript Author Manuscript Author Manuscript Author Manuscript

interact with G9A/GLP in undifferentiated ESCs (Mozzetta et al., 2014), and DNMT1 recognizes H3K9me2 through its interaction with UHRF1 (Rothbart et al., 2012). Since we see an interaction between EED, DNMT1 and UHRF1 in ESCs, we propose that this interaction occurs at promoters of gametogenic genes in the epiblast in order to establish a gametogenesis signature that is sustained in PGCs through continual recruitment of PRC2.

In summary, EED is required to prevent precocious PGC differentiation in response to sex-specific developmental signals during sex determination in the embryonic ovary and testis. Our results identify an expanded role for EED during PGC development beyond what was previously reported for EZH2, and provides an exciting glimpse into the complex epigenetic regulatory networks that govern PGC development, beginning in the epiblast.

Limitations of the Study

In order to show that DNMT1 and EED interact in the epiblast we used an *in vitro* model of the epiblast called Epiblast-Like Cells (EpiLC). While EpiLCs have a similar transcriptome to the post-implantation mouse epiblast, and can specify PGC-like cells *in vitro* (Hayashi et al., 2011), EpiLCs themselves are not generated in an egg cylinder embryo. In addition, this work revealed that EED is not responsible for maintaining DNA methylation at gametogenesis promoters following PGC specification *in vivo*. It remains to be determined whether the reciprocal is true.

STAR METHODS

RESOURCE AVAILABILITY

Lead contact—Further information and requests for resources and reagents should be directed to and will be fulfilled by the lead contact, Amander Clark (clarka@ucla.edu).

Materials availability—All unique/stable reagents generated in this study are available from the lead contact with a completed materials transfer agreement.

Data and code availability

- RNA-seq, single cell Smart-seq and whole genome bisulfite sequencing data have been deposited at GEO: GSE139413 and are publicly available as of the date of publication. Additionally, this paper analyzes existing, publicly available data. The accession numbers for these datasets are listed in the key resources table.
- There is no original code associated with this work.
- Any additional information required to reanalyze the data reported in this paper is available from the lead contact upon request.

EXPERIMENTAL MODEL AND SUBJECT DETAILS

Cell lines—V6.5 XY mouse embryonic stem cells (Novus Biologicals) used in the co-immunoprecipitation experiments were cultured in two different conditions, serum +Lif and 2i +Lif differentiated into EpiLCs. Serum +Lif culture media is KnockOut DEM

Author Manuscript Author Manuscript Author Manuscript Author Manuscript

(Invitrogen) supplemented with 15% Hyclone FBS (Thermo Fisher), 1000 U/mL ESGRO LIF (Fisher/Millipore), 55 μM Beta-mercaptoethanol (Invitrogen), Primocin (Invivogen), Pen/Strep/Glutamine (Invitrogen), and non-essential amino acids (Invitrogen) as per manufacturers instruction.

EpiLCs were differentiated from V6.5 XY mouse embryonic stem cells (Novus Biologicals) cultured in 2i +Lif conditions following the Hayashi et al., 2011 protocol. 2i +Lif culture media is equal parts DMEM/F12 without HEPES (gibco) and Neurobasal media (Gibco) supplemented with 3 μM CHIR99021 inhibitor (Stemgent), 0.5 μM PD0325901 inhibitor (Stemgent), 1000 U/mL ESGRO LIF (Fisher/Millipore), 110 μM Beta-mercaptoethanol (Invitrogen), N2 supplement (Gibco), B27 supplement (Gibco), Primocin (Invivogen), and Pen/Strep/Glutamine (Invitrogen) as per manufacturers instruction. EpiLC differentiation media is equal parts DMEM/F12 without HEPES (gibco) and Neurobasal media (Gibco) supplemented with 1% KSR (Gibco), 20 ng/mL Activin A human recombinant protein (Peprotech), 12 ng/mL bFGF (R&D Systems), 110 μM Beta-mercaptoethanol (Invitrogen), N2 supplement (Gibco), B27 supplement (Gibco), Primocin (Invivogen), and Pen/Strep/Glutamine (Invitrogen) as per manufacturers instruction.

All cells were grown at 37°C and are regularly screened to ensure they are mycoplasma negative.

Animal subjects—All animal experiments for this study were approved by the UCLA Institutional Animal Care and Use Committee, also known as the Chancellor's Animal Research Committee, in compliance with national laboratory animal care guidelines. All mice were housed in a standard facility with *ad libitum* access to irradiated standard mouse chow and water. All mouse lines were established from strains purchased from Jackson labs. $Eed^{fl/fl}$ mice were established in a B6;129 background and backcrossed with an inbred C57BL/6J strain (Yu et al., 2009). OG mice were established and maintained in a mixed B6;129 background (Lengner et al., 2007). BC mice were established in a B6CBAF1 background and backcrossed to C57BL/6J five times (Ohinata et al., 2005). Control and ECKO XY and XX embryos were obtained from crosses between 7-10 week old OG/OG; $Eed^{fl/fl}$ homozygous mothers and 7-30 week old BC; $Eed^{\Delta/+}$ heterozygous fathers. Impregnation was determined by detection of a vaginal plug on the morning after time-mating at which point the embryos were staged at E0.5. Embryos were harvested for microdissection at E10.5, E11.5, E12.5 and E13.5. Sex and genotype of the adult mice and embryos was confirmed by PCR. Control samples are OG/+; $Eed^{fl/+}$_and ECKO samples are BC/+; OG/+; $Eed^{\Delta/\Delta}$. Control and ECKO littermates of the same sex were used for each experiment whenever possible.

METHOD DETAILS

Immunofluorescence—Aorta-gonad-mesonephros (AGM) (E11.5) and gonads (E13.5) were extracted from the embryos via microdissection and fixed in 4% paraformaldehyde (Life Technologies) over night at 4°C. Following fixation, gonads were stored in 70% ethanol until sectioning. Gonads were embedded in paraffin wax and then cut into 5 μm sections. Sections were deparaffinized via immersion in xylene (Fisher Scientific)

Author Manuscript Author Manuscript Author Manuscript Author Manuscript

and rehydrated in an ethanol series. Antigen retrieval was performed at 95°C in either Tris-EDTA (10mM Trizma base (Sigma), 1mM EDTA (Sigma), 0.05% Tween-20 (Fisher Scientific) at a pH of 9.0) or Citrate (10 mM Sodium Citrate (Sigma), 0.05% Tween 20 at PH of 6) buffer for 40 minutes and then cooled back to room temperature (RT). Sections were washed with 0.2% Tween 20 in PBS (Fisher Scientific) (PBST), permeabilized in 0.5% Triton X-100 (Sigma) in PBS for 20 minutes at room temperature and then washed with PBST. Sections were blocked for 1 hour in 10% donkey serum (Fisher Scientific) in PBST. The primary antibody (Table S3) was added at the manufacturers recommended concentration in 2.5% donkey serum PBST and incubated overnight at 4°C in a humid chamber. Secondary antibody (Table S3) was added at a concentration of 1:200 in 2.5% donkey serum PBST and 1x DAPI (Fisher Scientific) for 1 hour at room temperature. Slides were mounted in Prolong Gold without DAPI mounting media (Invitrogen) and set to cure overnight at room temperature in a dark chamber before being transferred to 4°C for long term storage. All immunofluorescence sections were imaged on a Zeiss LSM 880 microscope as a Z stack which was then processed in Imaris (Bitplane) to trim the Z-stack to a one to two cell thickness (~5 μm) as a maximum intensity projection, adjust individual channels brightness for publication and quantify the images as described below.

For immunofluorescence staining, presence vs. absence of a mark was determined by identifying the TFAP2C+ (E11.5) or VASA+ (E13.5) PGCs and quantifying the amount of PGCs positive for the given mark by eye. The number of dual positive PGCs was divided by the total number of TFAP2C+/VASA+ PGCs to calculate the ratio for a set of sections. For all IF analysis, sections were analyzed from n≥3 embryonic mice of the appropriate condition. >50 PGCs were quantified for all analyses except the ECKO XX (>10 PGCs per sample) and E11.5 sections (>20 PGCs per sample) due to limited PGC cell number per section. Quantification of H3K27ac signal intensity within the PGC nucleus was performed in Imaris by first creating spots over the nuclei of VASA+/DAPI+ PGCs and VASA−/DAPI+ somatic cells. Mean H3K27ac signal intensity was measured over these spots and normalized for each image by taking the ratio of VASA+ PGC average nuclear signal over VASA− somatic nuclear signal. For the MILI analysis, due to higher background signal a mask over the VASA channel was created and then all MILI signal not under the mask was set to zero in order to only look at MILI signal within PGC cytoplasm. Significance for all IF data was calculated between ECKO and control via a two tailed, unequal variance T-test.

Sample Preparation for FACS—Aorta-gonad-mesonephros (AGM) (E10.5 and E11.5) and gonads (E12.5 and E13.5) were extracted from the embryos via microdissection and dissociated in 100 μL of 0.05% Trypsin-EDTA (Thermo Fisher Scientific) at 37°C for 5 minutes with additional minutes added if necessary. Quenched with 200 μL MEF media (10% FBS in DMEM) and spun down at 300xG to pellet the dissociated cells. The pellet was resuspended in 1% BSA (Sigma-Aldrich), passed through the cap strainer into a 5 mL Falcon Corning FACS tube and 7AAD (Fisher Scientific) was added to the solution prior to sorting. Only 7AAD −, GFP+ cells were sorted and used for further analysis. For bulk RNA sequencing, cells were sorted into 300 μL of RLT buffer (Qiagen) in a 1.5 mL Eppendorf tube and stored at −80 °C until library prep. For single cell RNA sequencing, individual XY

Author Manuscript Author Manuscript Author Manuscript Author Manuscript

and XX GFP+ cells were sorted into 2 μL of 0.2% Triton X-100 and 40 u/μL RNaseOut (Invitrogen) into a 96 well plate. Plates were sealed, spun down at 300xG for 1 minute and stored at −80°C until library prep. For whole genome bisulfite sequencing, all PGCs from XX E10.5 and E11.5 embryos were sorted into 0.2 mL PCR tubes containing 10 μL M-Digestion Buffer (Zymo) and 1 μL Proteinase K (Zymo), spun down and stored at −80°C until library prep.

Significance for FACS data was calculated via a two-tailed, unequal variance T-test. Linear regression analysis was performed based on the assumption that the rate of division across the PGC population in the gonad would be consistent and therefore linear on a log2 scale.

Genotyping—The head from each mouse embryo was collected for genotyping following extraction of the gonad and dissociated in 100 μL Modified Gitschier Buffer and 3 μL (1:33) Proteinase K (Sigma-Aldrich) at 55°C overnight followed by a 5 minute 95°C incubation to inactivate the enzyme. The sample was spun down to pellet the undigested debris and 1 μL of the supernatant was used for the genotyping PCR reactions. PCR products were run on a 2% Agarose gel for 1 hour at 100V. For a sexing PCR, XY embryos have two bands at roughly 300 bp and 280 bp, whereas XX only have a single band at 300 bp. Blimp1-cre PCR shows a single band at 200 bp if the transgene is present. Finally, the EED PCR has a control band at around 300 bp with a larger mutant band at around 350 bp. The sequence of all genotyping oligos is present in Table S4.

Bulk RNA-sequencing Analysis—Bulk RNA Libraries were made from sorted cells of the E11.5 XY and XX as well as E13.5 XY embryos. The cell lysate in RLT was thawed on ice and cleaned up using a Qiagen RNeasy Micro RNA kit. Following cleanup, the samples were converted to cDNA following the Ovation RNA-seq System V2 protocol (Nugen). 4.5 μL of RNA + 0.5 μL of ERCC (Thermo Fisher Scientific) spike in was converted to cDNA and purified with Agencourt RNAclean XP beads (Beckman Coulter). cDNA was amplified via the SPIA reaction, cleaned up using the Qiagen MinElute Reaction Cleanup Kit and eluted in 50 μL low EDTA TE buffer. Purified cDNA was quantified via Qubit and then sonicated into 200 bp fragments using a Covaris. Sonicated cDNA was purified using a Qiagen MinElute Reaction Cleanup Kit and eluted in 10 μL Low EDTA TE buffer. 8 μL of eluted cDNA was indexed using the Ovation Rapid DR Multiplex System with the indices L9–16. Following final repair, the indexed cDNA was purified using Agencourt RNAclean XP beads and eluted in 11 μL low EDTA TE buffer. Indexed libraries were quantified using the Kapa Library Quantification Kit for Illumina platforms (KAPA Biosystems). Libraries were submitted for sequencing in a single lane and sequenced as follows, E13.5 XY on the Illumina 2500 as single end 50 bp, E11.5 XX on the Illumina Hiseq 4000 as paired end 100 bp and the E11.5 XY on the Novaseq as paired end 50 bp.

The bulk RNA-sequencing reads were aligned to the mouse reference genome mm9 using HISAT2 (Kim et al., 2015) and mappability for each sample can be found in Table S5. The mRNA read counts of genes were computed using HTSeq (Anders et al., 2015). Genes that are expressed (read counts > 0) in at least one replicate in both control and ECKO are included for analysis. Normalization for sequencing depth and differential gene analysis was performed using edgeR (Robinson et al., 2010). Only genes with RPKM ≥10 in at

Author Manuscript Author Manuscript Author Manuscript Author Manuscript

least one sample after normalizing for sequencing depth were analyzed. Genes with ≥2-fold difference in expression and FDR < 5% were considered differentially expressed. Gene ontology analysis was performed using DAVID (Huang et al., 2009). All DEGs for bulk RNA-sequencing can be found in Table S1.

For the comparison of the E13.5 XY EED and DNMT1 conditional knockout upregulated DEGs, the RNA-sequencing datasets were first trimmed to remove all genes which are not expressed (read counts >0) in at least one replicate in both the control and mutant from each condition. Only genes with RPKM ≥10 in at least one samples after normalizing for sequencing depth were analyzed. Genes with ≥2-fold difference in expression and FDR <5% were considered differentially expressed. This ultimately led to a loss of 55 upregulated ECKO DEGs relative to the EED only analysis. Gene ontology analysis was performed using DAVID (Huang et al., 2009).

X Chromosome and TE Expression analysis—X chromosome over autosome expression ratio was calculated by dividing the mean RPKM normalized to sequencing depth of all X chromosome genes by the mean of all somatic genes. A two tailed, unequal variance T-test was then used to assess significance between the X/A ratio of control and ECKO PGCs. A hypergeometric test was used to evaluate the enrichment of the de-repressed genes with H3K27me3 in each chromosome. The test uses the hypergeometric distribution to calculate statistical significance of the enrichment of de-repressed gene promoters with H3K27me3 among all expressed genes on each chromosome. A p-value < 0.01 was considered to be statistically significant.

For TE analysis, raw reads were trimmed with cutadapt 1.18 (Martin, 2011) and trimmed reads with less than 30 bp were discarded. Retained reads were aligned to mm9 with STAR 2.7.0 (Dobin et al., 2013) setting --outFilterMultimapNmax 1000 --outSAMmultNmax 1. Reads aligned to TE were counted by multiBamCov in bedtools (Quinlan and Hall, 2010). RPKM was calculated by edgeR (Robinson et al., 2010).

Single Cell Smart RNA-sequencing Analysis—Single cell libraries were prepared according to the Smart-seq v4 library prep kit (Takara). Prior to the kit, plates were thawed and brought to 11.5 μL with 1 mM DNTP (Invitrogen) in nuclease free water. Kit protocol was followed exactly for reverse transcription. Following conversion, the libraries were amplified for 22 cycles and then purified using Agencourt Ampure XP beads (Beckman Coulter). The profile of each cDNA library was confirmed using a HS D5000 tape on an Agilent 2200 TapeStation. XX and XY cells were indexed following the Nextera XT DNA library prep kit and indexed with primer sets A and D (Illumina), respectively. Indexed libraries were pooled and purified using Agencourt XP beads and eluted in low EDTA TE buffer. The size profile of the purified eluate was confirmed using a D1000 tape on an Agilent 2200 TapeStation. The pooled libraries were multiplexed and sequenced on the Novaseq as paired end 100 bp.

Raw scRNA-sequencing reads were trimmed with cutadapt 1.18 (Martin, 2011). Trimmed reads with less than 30 bp were discarded. Retained reads were aligned to mm9 with STAR 2.7.0 (Dobin et al., 2013). Reads aligned to exons were counted by featureCount 2.0.1 (Liao

Author Manuscript Author Manuscript Author Manuscript Author Manuscript

et al., 2014) from the Subread package. Cells with at least 2000 genes and 0.8M reads were kept for further analysis. Downstream analyses including k-means clustering, DEG finding, and dimension reduction were performed with R packages SC3 (Kiselev et al., 2017) and Scater (McCarthy et al., 2017) and plotted with ggplot2 (Wickham, 2016). All DEGs for scRNA-sequencing can be found in Table S1.

Whole Genome Bisulfite Sequencing Analysis—Samples were thawed and brought to 20 μL with nuclease free water. Genomic DNA isolation and bisulfite conversion was performed as per the EZ DNA Methylation-Direct Kit (Zymo). Following desulfonation, samples were indexed following the Pico Methyl-seq Library Prep Kit (Zymo) with a few modifications due to the low input cell number. For the initial amplification, only 1 μL of primer was added. Additionally, during library amplification 10 PCR cycles were performed. Following indexing and purification, samples were run on the Agilent 2200 TapeStation to ensure proper size profile using a D1000 tape and then sequenced on a Novaseq as paired end 100 bp.

Raw WGBS reads were trimmed with cutadapt 1.18 (Martin, 2011) and trimmed reads with less than 30 bp were discarded. Retained reads were aligned to mm9 with BS-Seeker 2 (Guo et al., 2013). Duplicated reads were removed from .bam file with picard_tools (Broad Institute, 2020). Cytosines and reverse complimented guanines with coverage ≥ 4 were retained and calculated for average CG methylation level.

Promoter Methylation Analysis—The E6.5 and E11.5 whole genome bisulfite sequencing datasets were downloaded from European Nucleotide Archive under the accession number ERP001953 (Seisenberger et al., 2012). The reads were mapped against the mouse reference genome mm9 using BS-Seeker 2 (Guo et al., 2013). Genome-wide DNA methylation profiles were generated by determining methylation levels for each cytosine in the genome. The methylation level per cytosine serves as an estimate of the percentage of cells that have a methylated cytosine at a specific locus. We only included cytosines that are covered by at least three reads. The promoter region is defined as the region between −2,000 bp<TSS<+500 bp. Methylation over a promoter region was calculated for each CG in the region and then these individual values were averaged to give a representative value for the promoter region. Analysis of all promoters based on %CG methylation can be found in Table S2.

H3K27me3 and CpG Classification—ChIP-seq data of H3K27me3 in mouse Epiblast at E6.5 was downloaded from GSE104243 (Yang et al., 2018), H3K27me3 in mouse PGCs at E11.5 was downloaded from GEO accession GSE46396 (Sachs et al., 2013), and H3K27m3 in mouse PGCs at E13.5 was downloaded from GEO accession GSE60377 (Liu et al., 2014). Reads were aligned to the mouse reference genome mm9 using bowtie2 (Langmead and Salzberg, 2012) and the uniquely aligned reads were retained using SAMtools (Li et al., 2009). The E6.5, E11.5 and E13.5 ChIP-seq data were compared between H3K27me3 ChIP-seq and their corresponding control (input or H3) at promoters (−2000 to +500 of TSS) using edgeR (Robinson et al., 2010). The comparison considered the control, replicates, and statistical significance. The promoters with q-value < 0.05 and fold-change ≥ 2 are considered as H3K27me3 enriched promoters. The promoters on the

Author Manuscript Author Manuscript Author Manuscript Author Manuscript

sex chromosomes were excluded from this analysis. Presence or absence of an H3K27me3 enriched promoter at E6.5 and E11.5 was used to classify the promoters into one of four categories. CpG classification for all promoters was performed according to (Weber et al., 2007), updating the CpG cutoffs for the mouse genome as per (Mohn et al., 2008). Analysis of DEGs based on H3K27me3 promoter content can be found in Table S1 and all promoters in Table S2. Analysis of all promoters CpG content can be found in Table S2.

Significance for the distribution of %CG methylation within the pre-existing late demethylating promoters was determined by first classifying all promoters as either “High” (≥mean%) or “Low” (<mean%) for the time point. Hypergeometric testing was performed to identify enrichment or depletion for %CG methylation within the pre-existing or acquired promoters relative to their abundance within the genome at a given embryonic time point. Additionally, hypergeometric testing was used to identify the enrichment for each CpG content category (LCP, ICP, HCP) within the pre-existing and acquired promoters using the relative distribution in all promoters as the population.

Native Co-Immunoprecipitation—Mouse embryonic stem cells (ESC) were cultured in serum +Lif. EpiLC were differentiated from mouse embryonic stem cells cultured in 2i +Lif conditions following the Hayashi et al., 2011 protocol. 3 million cells were harvested in cold PBS and lysed with 130 mM NaCl, 1% NP-40 (Sigma), 1 mM EDTA (Thermo), and 25 mM Hepes (Thermo) in the presence of 1x HALT protease inhibitor cocktail (Invitrogen). Lysate was agitated for 30 minutes on a rotator at 4°C and then centrifuged at 4°C to pellet the cellular debris. Supernatant was precleared with protein G dynabeads (Thermo). Pulldown was performed by adding 500 μg of protein lysate to 5 μg of rabbit anti-DNMT1 (ab188453), mouse anti-DNMT1 (NB100-56519) or mouse anti-EED (05-132) antibody (Table S3) bound to protein A (rabbit) or G (mouse) dynabeads at 4°C for 1 hour on a rotator. A species matched negative control IgG (Mouse (5415) or Rabbit (ab27478)) was performed in parallel using 500 μg of the same input. Following incubation, beads were washed with lysis buffer 3 times. Beads were then resuspended in 40 μL 1x LDS (Thermo) and 1x NuPAGE reducing agent (Thermo) and boiled for 10 minutes at 95 °C to release the protein. 10 μL (1/4) of eluted IP supernatant was loaded onto a 4-12% Bis-Tris gel (Thermo) alongside 5 μg input and 10 μL (1/4) of eluted IgG supernatant. Proteins were transferred to a PVDF membrane using the Biorad Trans-Blot Turbo system, blocked with TBST+5% milk for 30 minutes, cut into strips and then exposed to appropriate primary antibodies (Table S3) at 4°C. The strips were then washed with TBST for 5 minutes 5 times, blocked for 10 minutes with TBST+5% milk and then incubated with secondary antibodies (Table S3) in TBST+5% milk for 1 hour at room temperature on a rocker. Membranes were washed in TBST for 5 minutes 5 times, exposed to ECL reagent (Thermo) and then imaged using a BioRad Chemidoc. For all co-IP analysis, an independent replicate is considered an independent pulldown. All replicate and uncropped blots can be found in Data S1.

QUANTIFICATION AND STATISTICAL ANALYSIS

Statistical tests and cutoffs used for each analysis are reported in each methods subsection. All information on replicate numbers and error bars is present in the figure legends and methods. $p<0.05$ was considered significant for all tests, except in bulk RNA sequencing

Author Manuscript Author Manuscript Author Manuscript Author Manuscript

results which were considered significant if the FDR was <0.05 and X chromosome Hypergeometric testing where a p<0.01 was considered significant.

Supplementary Material

Refer to Web version on PubMed Central for supplementary material.

Acknowledgements

The authors would like to thank the UCLA BSCRC flow cytometry core, the UCLA BSCRC Sequencing core, and the UCLA MCDB/BSCRC Microscopy Core. We would also like to thank Dr. Jesse Zamudio for his expert guidance on statistical analyses used throughout this study. Funding for this project provided by NIH/NICHD 2 R01 HD058047, a Ruth L. Kirschstein National Research Service Award GM007185, the UCLA Eli and Edythe Broad Center of Regenerative Medicine and Stem Cell Research Training Program and the Rose Hill Foundation Science and Engineering Scholarship. P.Y.C. was supported by grants from Academia Sinica and Ministry of Science and Technology Taiwan (107-2633-B-001-001 and 108-2313-B-001-013-MY3).

References

Anders S, Pyl PT, and Huber W (2015). HTSeq—a Python framework to work with high-throughput sequencing data. Bioinformatics 31, 166–169. 10.1093/bioinformatics/btu638. [PubMed: 25260700]

Aravin AA, Sachidanandam R, Bourc'his D, Schaefer C, Pezic D, Toth KF, Bestor T, and Hannon GJ (2008). A piRNA pathway primed by individual transposons is linked to de novo DNA methylation in mice. Mol. Cell 31, 785–799. 10.1016/j.molcel.2008.09.003. [PubMed: 18922463]

Baltus AE, Menke DB, Hu Y-C, Goodheart ML, Carpenter AE, de Rooij DG, and Page DC (2006). In germ cells of mouse embryonic ovaries, the decision to enter meiosis precedes premeiotic DNA replication. Nat Genet 38, 1430–1434. 10.1038/ng1919. [PubMed: 17115059]

Bartke T, Vermeulen M, Xhemalce B, Robson SC, Mann M, and Kouzarides T (2010). Nucleosome-Interacting Proteins Regulated by DNA and Histone Methylation. Cell 143, 470–484. 10.1016/j.cell.2010.10.012. [PubMed: 21029866]

Boulares AH, Yakovlev AG, Ivanova V, Stoica BA, Wang G, Iyer S, and Smulson M (1999). Role of Poly(ADP-ribose) Polymerase (PARP) Cleavage in Apoptosis CASPASE 3-RESISTANT PARP MUTANT INCREASES RATES OF APOPTOSIS IN TRANSFECTED CELLS. J. Biol. Chem 274, 22932–22940. 10.1074/jbc.274.33.22932. [PubMed: 10438458]

Bracken AP, Dietrich N, Pasini D, Hansen KH, and Helin K (2006). Genome-wide mapping of Polycomb target genes unravels their roles in cell fate transitions. Genes Dev. 20, 1123–1136. 10.1101/gad.381706. [PubMed: 16618801]

Broad Institute (2020). Picard Toolkit. Broad Institute, Github Repository. http://broadinstitute.github.io/picard/

Cao Q, Wang X, Zhao M, Yang R, Malik R, Qiao Y, Poliakov A, Yocum AK, Li Y, Chen W, et al. (2014). The central role of EED in the orchestration of polycomb group complexes. Nat Commun 5, 3127. 10.1038/ncomms4127. [PubMed: 24457600]

Chen F, Zhang Q, Deng X, Zhang X, Chen C, Lv D, Li Y, Li D, Zhang Y, Li P, et al. (2018). Conflicts of CpG density and DNA methylation are proximally and distally involved in gene regulation in human and mouse tissues. Epigenetics 13, 721–741. 10.1080/15592294.2018.1500057. [PubMed: 30009687]

Dewannieux M, Dupressoir A, Harper F, Pierron G, and Heidmann T (2004). Identification of autonomous IAP LTR retrotransposons mobile in mammalian cells. Nature Genetics 36, 534–539. 10.1038/ng1353. [PubMed: 15107856]

Dobin A, Davis CA, Schlesinger F, Drenkow J, Zaleski C, Jha S, Batut P, Chaisson M, and Gingeras TR (2013). STAR: ultrafast universal RNA-seq aligner. Bioinformatics 29, 15–21. 10.1093/bioinformatics/bts635. [PubMed: 23104886]

Author Manuscript Author Manuscript Author Manuscript Author Manuscript

Endoh M, Endo TA, Shinga J, Hayashi K, Farcas A, Ma K-W, Ito S, Sharif J, Endoh T, Onaga N, et al. (2017). PCGF6-PRC1 suppresses premature differentiation of mouse embryonic stem cells by regulating germ cell-related genes. ELife 6, e21064. 10.7554/eLife.21064. [PubMed: 28304275]

Gerdes J, Schwab U, Lemke H, and Stein H (1983). Production of a mouse monoclonal antibody reactive with a human nuclear antigen associated with cell proliferation. Int. J. Cancer 31, 13–20. 10.1002/ijc.2910310104. [PubMed: 6339421]

Ginsburg M, Snow MH, and McLaren A (1990). Primordial germ cells in the mouse embryo during gastrulation. Development 110, 521–528. . [PubMed: 2133553]

Guibert S, Forné T, and Weber M (2012). Global profiling of DNA methylation erasure in mouse primordial germ cells. Genome Res 22, 633–641. 10.1101/gr.130997.111. [PubMed: 22357612]

Guo W, Fiziev P, Yan W, Cokus S, Sun X, Zhang MQ, Chen P-Y, and Pellegrini M (2013). BS-Seeker2: a versatile aligning pipeline for bisulfite sequencing data. BMC Genomics 14, 774. 10.1186/1471-2164-14-774. [PubMed: 24206606]

Hackett JA, Sengupta R, Zylicz JJ, Murakami K, Lee C, Down TA, and Surani MA (2013). Germline DNA Demethylation Dynamics and Imprint Erasure Through 5-Hydroxymethylcytosine. Science 339, 448–452. 10.1126/science.1229277. [PubMed: 23223451]

Haggerty C, Kretzmer H, Riemenschneider C, Kumar AS, Mattei AL, Bailly N, Gottfreund J, Giesselmann P, Weigert R, Brändl B, et al. (2021). Dnmt1 has de novo activity targeted to transposable elements. Nat Struct Mol Biol 28, 594–603. 10.1038/s41594-021-00603-8. [PubMed: 34140676]

Hajkova P, Erhardt S, Lane N, Haaf T, El-Maarri O, Reik W, Walter J, and Surani MA (2002). Epigenetic reprogramming in mouse primordial germ cells. Mech. Dev 117, 15–23. 10.1016/s0925-4773(02)00181-8. [PubMed: 12204247]

Hargan-Calvopina J, Taylor S, Cook H, Hu Z, Lee SA, Yen M-R, Chiang Y-S, Chen P-Y, and Clark AT (2016). Stage-Specific Demethylation in Primordial Germ Cells Safeguards against Precocious Differentiation. Dev. Cell 39, 75–86. 10.1016/j.devcel.2016.07.019. [PubMed: 27618282]

Hayashi K, Ohta H, Kurimoto K, Aramaki S, and Saitou M (2011). Reconstitution of the mouse germ cell specification pathway in culture by pluripotent stem cells. Cell 146, 519–532. 10.1016/j.cell.2011.06.052. [PubMed: 21820164]

Heeringen SJ van, Akkers RC, Kruijsbergen I van, Arif MA, Hanssen LLP, Sharifi N, and Veenstra GJC (2014). Principles of nucleation of H3K27 methylation during embryonic development. Genome Res. 24, 401–410. 10.1101/gr.159608.113. [PubMed: 24336765]

Hill PWS, Leitch HG, Requena CE, Sun Z, Amouroux R, Roman-Trufero M, Borkowska M, Terragni J, Vaisvila R, Linnett S, et al. (2018). Epigenetic reprogramming enables the primordial germ cell-to-gonocyte transition. Nature 555, 392–396. 10.1038/nature25964. [PubMed: 29513657]

Huang DW, Sherman BT, and Lempicki RA (2009). Bioinformatics enrichment tools: paths toward the comprehensive functional analysis of large gene lists. Nucleic Acids Res 37, 1–13. 10.1093/nar/gkn923. [PubMed: 19033363]

Huang T-C, Wang Y-F, Vazquez-Ferrer E, Theofel I, Requena CE, Hanna CW, Kelsey G, and Hajkova P (2021). Sex-specific chromatin remodelling safeguards transcription in germ cells. Nature 1–6. 10.1038/s41586-021-04208-5.

Jadhav U, Manieri E, Nalapareddy K, Madha S, Chakrabarti S, Wucherpfennig K, Barefoot M, and Shivdasani RA (2020). Replicational Dilution of H3K27me3 in Mammalian Cells and the Role of Poised Promoters. Molecular Cell 78, 141–151.e5. 10.1016/j.molcel.2020.01.017. [PubMed: 32027840]

Jameson SA, Natarajan A, Cool J, DeFalco T, Maatouk DM, Mork L, Munger SC, and Capel B (2012). Temporal Transcriptional Profiling of Somatic and Germ Cells Reveals Biased Lineage Priming of Sexual Fate in the Fetal Mouse Gonad. PLOS Genetics 8, e1002575. 10.1371/journal.pgen.1002575. [PubMed: 22438826]

Kim D, Langmead B, and Salzberg SL (2015). HISAT: a fast spliced aligner with low memory requirements. Nat. Methods 12, 357–360. 10.1038/nmeth.3317. [PubMed: 25751142]

Kim S, Günesdogan U, Zylicz JJ, Hackett JA, Cougot D, Bao S, Lee C, Dietmann S, Allen GE, Sengupta R, et al. (2014). PRMT5 Protects Genomic Integrity during Global DNA Demethylation

Author Manuscript Author Manuscript Author Manuscript Author Manuscript

in Primordial Germ Cells and Preimplantation Embryos. Mol Cell 56, 564–579. 10.1016/j.molcel.2014.10.003. [PubMed: 25457166]

King AD, Huang K, Rubbi L, Liu S, Wang C-Y, Wang Y, Pellegrini M, and Fan G (2016). Reversible Regulation of Promoter and Enhancer Histone Landscape by DNA Methylation in Mouse Embryonic Stem Cells. Cell Rep 17, 289–302. 10.1016/j.celrep.2016.08.083. [PubMed: 27681438]

Kiselev VYu., Kirschner K, Schaub MT, Andrews T, Yiu A, Chandra T, Natarajan KN, Reik W, Barahona M, Green AR, et al. (2017). SC3-consensus clustering of single-cell RNA-Seq data. Nat Methods 14, 483–486. 10.1038/nmeth.4236. [PubMed: 28346451]

Kobayashi H, Sakurai T, Miura F, Imai M, Mochiduki K, Yanagisawa E, Sakashita A, Wakai T, Suzuki Y, Ito T, et al. (2013). High-resolution DNA methylome analysis of primordial germ cells identifies gender-specific reprogramming in mice. Genome Res 23, 616–627. 10.1101/gr.148023.112. [PubMed: 23410886]

Kuzmichev A, Nishioka K, Erdjument-Bromage H, Tempst P, and Reinberg D (2002). Histone methyltransferase activity associated with a human multiprotein complex containing the Enhancer of Zeste protein. Genes Dev 16, 2893–2905. 10.1101/gad.1035902. [PubMed: 12435631]

Langmead B, and Salzberg SL (2012). Fast gapped-read alignment with Bowtie 2. Nat. Methods 9, 357–359. 10.1038/nmeth.1923. [PubMed: 22388286]

Lengner CJ, Camargo FD, Hochedlinger K, Welstead GG, Zaidi S, Gokhale S, Scholer HR, Tomilin A, and Jaenisch R (2007). Oct4 Expression Is Not Required for Mouse Somatic Stem Cell Self-Renewal. Cell Stem Cell 1, 403–415. 10.1016/j.stem.2007.07.020. [PubMed: 18159219]

Lesch BJ, Dokshin GA, Young RA, McCarrey JR, and Page DC (2013). A set of genes critical to development is epigenetically poised in mouse germ cells from fetal stages through completion of meiosis. Proc Natl Acad Sci U S A 110, 16061–16066. 10.1073/pnas.1315204110. [PubMed: 24043772]

Li H, Handsaker B, Wysoker A, Fennell T, Ruan J, Homer N, Marth G, Abecasis G, Durbin R, and 1000 Genome Project Data Processing Subgroup (2009). The Sequence Alignment/Map format and SAMtools. Bioinformatics 25, 2078–2079. 10.1093/bioinformatics/btp352. [PubMed: 19505943]

Li Y, Zheng H, Wang Q, Zhou C, Wei L, Liu X, Zhang W, Zhang Y, Du Z, Wang X, et al. (2018). Genome-wide analyses reveal a role of Polycomb in promoting hypomethylation of DNA methylation valleys. Genome Biology 19, 18. 10.1186/s13059-018-1390-8. [PubMed: 29422066]

Liao Y, Smyth GK, and Shi W (2014). featureCounts: an efficient general purpose program for assigning sequence reads to genomic features. Bioinformatics 30, 923–930. 10.1093/bioinformatics/btt656. [PubMed: 24227677]

Liu M, Zhu Y, Xing F, Liu S, Xia Y, Jiang Q, and Qin J (2020). The polycomb group protein PCGF6 mediates germline gene silencing by recruiting histone-modifying proteins to target gene promoters. J. Biol. Chem 295, 9712–9724. 10.1074/jbc.RA119.012121. [PubMed: 32482889]

Liu Q, Wang G, Li Q, Jiang W, Kim J, Wang R, Zhu S, Wang X, Yan L, Yi Y, et al. (2019). Polycomb group proteins EZH2 and EED directly regulate androgen receptor in advanced prostate cancer. Int. J. Cancer 145, 415–426. 10.1002/ijc.32118. [PubMed: 30628724]

Liu S, Brind'Amour J, Karimi MM, Shirane K, Bogutz A, Lefebvre L, Sasaki H, Shinkai Y, and Lorincz MC (2014). Setdb1 is required for germline development and silencing of H3K9me3-marked endogenous retroviruses in primordial germ cells. Genes Dev. 28, 2041–2055. 10.1101/gad.244848.114. [PubMed: 25228647]

Lopes SMC de S, Hayashi K, Shovlin TC, Mifsud W, Surani MA, and McLaren A (2008). X Chromosome Activity in Mouse XX Primordial Germ Cells. PLOS Genetics 4, e30. 10.1371/journal.pgen.0040030. [PubMed: 18266475]

Mallol A, Guirola M, and Payer B (2019). PRDM14 controls X-chromosomal and global epigenetic reprogramming of H3K27me3 in migrating mouse primordial germ cells. Epigenetics & Chromatin 12, 38. 10.1186/s13072-019-0284-7. [PubMed: 31221220]

Martin M (2011). Cutadapt removes adapter sequences from high-throughput sequencing reads. EMBnet.Journal 17, 10–12. 10.14806/ej.17.1.200.

Author Manuscript Author Manuscript Author Manuscript Author Manuscript

McCarrey JR, and Dilworth DD (1992). Expression of Xist in mouse germ cells correlates with X–chromosome inactivation. Nature Genetics 2, 200–203. 10.1038/ng1192-200. [PubMed: 1345169]

McCarthy DJ, Campbell KR, Lun ATL, and Wills QF (2017). Scater: pre-processing, quality control, normalization and visualization of single-cell RNA-seq data in R. Bioinformatics 33, 1179–1186. 10.1093/bioinformatics/btw777. [PubMed: 28088763]

Mendenhall EM, Koche RP, Truong T, Zhou VW, Issac B, Chi AS, Ku M, and Bernstein BE (2010). GC-Rich Sequence Elements Recruit PRC2 in Mammalian ES Cells. PLOS Genetics 6, e1001244. 10.1371/journal.pgen.1001244. [PubMed: 21170310]

van Mierlo G, Dirks RAM, De Clerck L, Brinkman AB, Huth M, Kloet SL, Saksouk N, Kroeze LI, Willems S, Farlik M, et al. (2019). Integrative Proteomic Profiling Reveals PRC2-Dependent Epigenetic Crosstalk Maintains Ground-State Pluripotency. Cell Stem Cell 24, 123–137.e8. 10.1016/j.stem.2018.10.017. [PubMed: 30472157]

Mohn F, Weber M, Rebhan M, Roloff TC, Richter J, Stadler MB, Bibel M, and Schübeler D (2008). Lineage-Specific Polycomb Targets and De Novo DNA Methylation Define Restriction and Potential of Neuronal Progenitors. Molecular Cell 30, 755–766. 10.1016/j.molcel.2008.05.007. [PubMed: 18514006]

Montgomery ND, Yee D, Montgomery SA, and Magnuson T (2007). Molecular and functional mapping of EED motifs required for PRC2-dependent histone methylation. J Mol Biol 374, 1145–1157. 10.1016/j.jmb.2007.10.040. [PubMed: 17997413]

Mozzetta C, Pontis J, Fritsch L, Robin P, Portoso M, Proux C, Margueron R, and Ait-Si-Ali S (2014). The Histone H3 Lysine 9 Methyltransferases G9a and GLP Regulate Polycomb Repressive Complex 2-Mediated Gene Silencing. Molecular Cell 53, 277–289. 10.1016/j.molcel.2013.12.005. [PubMed: 24389103]

Murphy PJ, Cipriany BR, Wallin CB, Ju CY, Szeto K, Hagarman JA, Benitez JJ, Craighead HG, and Soloway PD (2013). Single-molecule analysis of combinatorial epigenomic states in normal and tumor cells. PNAS 110, 7772–7777. 10.1073/pnas.1218495110. [PubMed: 23610441]

Napoles M. de, Nesterova T, and Brockdorff N (2007). Early Loss of Xist RNA Expression and Inactive X Chromosome Associated Chromatin Modification in Developing Primordial Germ Cells. PLOS ONE 2, e860. 10.1371/journal.pone.0000860. [PubMed: 17848991]

de Napoles M, Mermoud JE, Wakao R, Tang YA, Endoh M, Appanah R, Nesterova TB, Silva J, Otte AP, Vidal M, et al. (2004). Polycomb Group Proteins Ring1A/B Link Ubiquitylation of Histone H2A to Heritable Gene Silencing and X Inactivation. Developmental Cell 7, 663–676. 10.1016/j.devcel.2004.10.005. [PubMed: 15525528]

Ng J-H, Kumar V, Muratani M, Kraus P, Yeo J-C, Yaw L-P, Xue K, Lufkin T, Prabhakar S, and Ng H-H (2013). In vivo epigenomic profiling of germ cells reveals germ cell molecular signatures. Dev. Cell 24, 324–333. 10.1016/j.devcel.2012.12.011. [PubMed: 23352811]

Ohinata Y, Payer B, O'Carroll D, Ancelin K, Ono Y, Sano M, Barton SC, Obukhanych T, Nussenzweig M, Tarakhovsky A, et al. (2005). Blimp1 is a critical determinant of the germ cell lineage in mice. Nature 436, 207–213. 10.1038/nature03813. [PubMed: 15937476]

Pasini D, Malatesta M, Jung HR, Walfridsson J, Willer A, Olsson L, Skotte J, Wutz A, Porse B, Jensen ON, et al. (2010). Characterization of an antagonistic switch between histone H3 lysine 27 methylation and acetylation in the transcriptional regulation of Polycomb group target genes. Nucleic Acids Res 38, 4958–4969. 10.1093/nar/gkq244. [PubMed: 20385584]

Prokopuk L, Stringer JM, Hogg K, Elgass KD, and Western PS (2017). PRC2 is required for extensive reorganization of H3K27me3 during epigenetic reprogramming in mouse fetal germ cells. Epigenetics & Chromatin 10, 7. 10.1186/s13072-017-0113-9. [PubMed: 28239420]

Prokopuk L, Hogg K, and Western PS (2018). Pharmacological inhibition of EZH2 disrupts the female germline epigenome. Clinical Epigenetics 10, 33. 10.1186/s13148-018-0465-4. [PubMed: 29515677]

Quinlan AR, and Hall IM (2010). BEDTools: a flexible suite of utilities for comparing genomic features. Bioinformatics 26, 841–842. 10.1093/bioinformatics/btq033. [PubMed: 20110278]

Richardson SR, Gerdes P, Gerhardt DJ, Sanchez-Luque FJ, Bodea G-O, Muñoz-Lopez M, Jesuadian JS, Kempen M-JHC, Carreira PE, Jeddeloh JA, et al. (2017). Heritable L1 retrotransposition

Author Manuscript Author Manuscript Author Manuscript Author Manuscript

in the mouse primordial germline and early embryo. Genome Res. 27, 1395–1405. 10.1101/gr.219022.116. [PubMed: 28483779]

Robinson MD, McCarthy DJ, and Smyth GK (2010). edgeR: a Bioconductor package for differential expression analysis of digital gene expression data. Bioinformatics 26, 139–140. 10.1093/bioinformatics/btp616. [PubMed: 19910308]

Rothbart SB, Krajewski K, Nady N, Tempel W, Xue S, Badeaux AI, Barsyte-Lovejoy D, Martinez JY, Bedford MT, Fuchs SM, et al. (2012). Association of UHRF1 with H3K9 methylation directs the maintenance of DNA methylation. Nat Struct Mol Biol 19, 1155–1160. 10.1038/nsmb.2391. [PubMed: 23022729]

Sachs M, Onodera C, Blaschke K, Ebata KT, Song JS, and Ramalho-Santos M (2013). Bivalent Chromatin Marks Developmental Regulatory Genes in the Mouse Embryonic Germline in Vivo. Cell Rep 3, 1777–1784. 10.1016/j.celrep.2013.04.032. [PubMed: 23727241]

Saitou M, and Yamaji M (2012). Primordial Germ Cells in Mice. Cold Spring Harb Perspect Biol 4, a008375. 10.1101/cshperspect.a008375. [PubMed: 23125014]

Sangrithi MN, Royo H, Mahadevaiah SK, Ojarikre O, Bhaw L, Sesay A, Peters AHFM, Stadler M, and Turner JMA (2017). Non-Canonical and Sexually Dimorphic X Dosage Compensation States in the Mouse and Human Germline. Developmental Cell 40, 289–301.e3. 10.1016/j.devcel.2016.12.023. [PubMed: 28132849]

Schuettengruber B, Bourbon H-M, Di Croce L, and Cavalli G (2017). Genome Regulation by Polycomb and Trithorax: 70 Years and Counting. Cell 171, 34–57. 10.1016/j.cell.2017.08.002. [PubMed: 28938122]

Seisenberger S, Andrews S, Krueger F, Arand J, Walter J, Santos F, Popp C, Thienpont B, Dean W, and Reik W (2012). The Dynamics of Genome-wide DNA Methylation Reprogramming in Mouse Primordial Germ Cells. Mol Cell 48, 849–862. 10.1016/j.molcel.2012.11.001. [PubMed: 23219530]

Seki Y, Hayashi K, Itoh K, Mizugaki M, Saitou M, and Matsui Y (2005). Extensive and orderly reprogramming of genome-wide chromatin modifications associated with specification and early development of germ cells in mice. Dev. Biol 278, 440–458. 10.1016/j.ydbio.2004.11.025. [PubMed: 15680362]

Soh YQS, Mikedis MM, Kojima M, Godfrey AK, Rooij D.G. de, and Page DC (2017). Meioc maintains an extended meiotic prophase I in mice. PLOS Genetics 13, e1006704. 10.1371/journal.pgen.1006704. [PubMed: 28380054]

Stringer JM, Forster SC, Qu Z, Prokopuk L, O'Bryan MK, Gardner DK, White SJ, Adelson D, and Western PS (2018). Reduced PRC2 function alters male germline epigenetic programming and paternal inheritance. BMC Biology 16, 104. 10.1186/s12915-018-0569-5. [PubMed: 30236109]

Sugimoto M, and Abe K (2007). X Chromosome Reactivation Initiates in Nascent Primordial Germ Cells in Mice. PLOS Genetics 3, e116. 10.1371/journal.pgen.0030116. [PubMed: 17676999]

Traut W, Endl E, Scholzen T, Gerdes J, and Winking H (2002). The temporal and spatial distribution of the proliferation associated Ki-67 protein during female and male meiosis. Chromosoma 111, 156–164. 10.1007/s00412-002-0202-8. [PubMed: 12355204]

Wang Q, Yu G, Ming X, Xia W, Xu X, Zhang Y, Zhang W, Li Y, Huang C, Xie H, et al. (2020). Imprecise DNMT1 activity coupled with neighbor-guided correction enables robust yet flexible epigenetic inheritance. Nature Genetics 52, 828–839. 10.1038/s41588-020-0661-y. [PubMed: 32690947]

Weber M, Hellmann I, Stadler MB, Ramos L, Pääbo S, Rebhan M, and Schübeler D (2007). Distribution, silencing potential and evolutionary impact of promoter DNA methylation in the human genome. Ng 39, 457–466. 10.1038/ng1990.

Western PS, Miles DC, van den, Bergen JA Burton M, and Sinclair AH (2008). Dynamic Regulation of Mitotic Arrest in Fetal Male Germ Cells. STEM CELLS 26, 339–347. 10.1634/stemcells.2007-0622. [PubMed: 18024419]

Wickham H (2016). ggplot2: Elegant Graphics for Data Analysis (Springer International Publishing).

Wu H, D'Alessio AC, Ito S, Xia K, Wang Z, Cui K, Zhao K, Eve Sun Y, and Zhang Y (2011). Dual functions of Tet1 in transcriptional regulation in mouse embryonic stem cells. Nature 473, 389–393. 10.1038/nature09934. [PubMed: 21451524]

Author Manuscript Author Manuscript Author Manuscript Author Manuscript

Yamaguchi S, Hong K, Liu R, Inoue A, Shen L, Zhang K, and Zhang Y (2013). Dynamics of 5-methylcytosine and 5-hydroxymethylcytosine during germ cell reprogramming. Cell Res. 23, 329–339. 10.1038/cr.2013.22. [PubMed: 23399596]

Yang X, Hu B, Hou Y, Qiao Y, Wang R, Chen Y, Qian Y, Feng S, Chen J, Liu C, et al. (2018). Silencing of developmental genes by H3K27me3 and DNA methylation reflects the discrepant plasticity of embryonic and extraembryonic lineages. Cell Res 28, 593–596. 10.1038/s41422-018-0010-1. [PubMed: 29463899]

Yokobayashi S, Liang C-Y, Kohler H, Nestorov P, Liu Z, Vidal M, van Lohuizen M, Roloff TC, and Peters AHFM (2013). PRC1 coordinates timing of sexual differentiation of female primordial germ cells. Nature 495, 236–240. 10.1038/nature11918. [PubMed: 23486062]

Yu M, Riva L, Xie H, Schindler Y, Moran TB, Cheng Y, Yu D, Hardison R, Weiss MJ, Orkin SH, et al. (2009). Insights into GATA-1-mediated gene activation versus repression via genome-wide chromatin occupancy analysis. Mol. Cell 36, 682–695. 10.1016/j.molcel.2009.11.002. [PubMed: 19941827]

Zhao W, Tong H, Huang Y, Yan Y, Teng H, Xia Y, Jiang Q, and Qin J (2017). Essential Role for Polycomb Group Protein Pcgf6 in Embryonic Stem Cell Maintenance and a Noncanonical Polycomb Repressive Complex 1 (PRC1) Integrity. J. Biol. Chem 292, 2773–2784. 10.1074/jbc.M116.763961. [PubMed: 28049731]

Zhao Z-H, Ma J-Y, Meng T-G, Wang Z-B, Yue W, Zhou Q, Li S, Feng X, Hou Y, Schatten H, et al. (2020). Single-cell RNA sequencing reveals the landscape of early female germ cell development. The FASEB Journal 34, 12634–12645. 10.1096/fj.202001034RR. [PubMed: 32716582]

Zheng H, Huang B, Zhang B, Xiang Y, Du Z, Xu Q, Li Y, Wang Q, Ma J, Peng X, et al. (2016). Resetting Epigenetic Memory by Reprogramming of Histone Modifications in Mammals. Molecular Cell 63, 1066–1079. 10.1016/j.molcel.2016.08.032. [PubMed: 27635762]

Author Manuscript Author Manuscript Author Manuscript Author Manuscript

Highlights

- EED regulates the timing of PGC differentiation in the embryonic gonad
- X Decompensation in XY PGCs is regulated by EED
- Gametogenesis promoters begin with H3K27me3 and DNA methylation in the epiblast
- DNMT1 and EED interact in embryonic stem cells and epiblast-like cells

Author Manuscript Author Manuscript Author Manuscript Author Manuscript

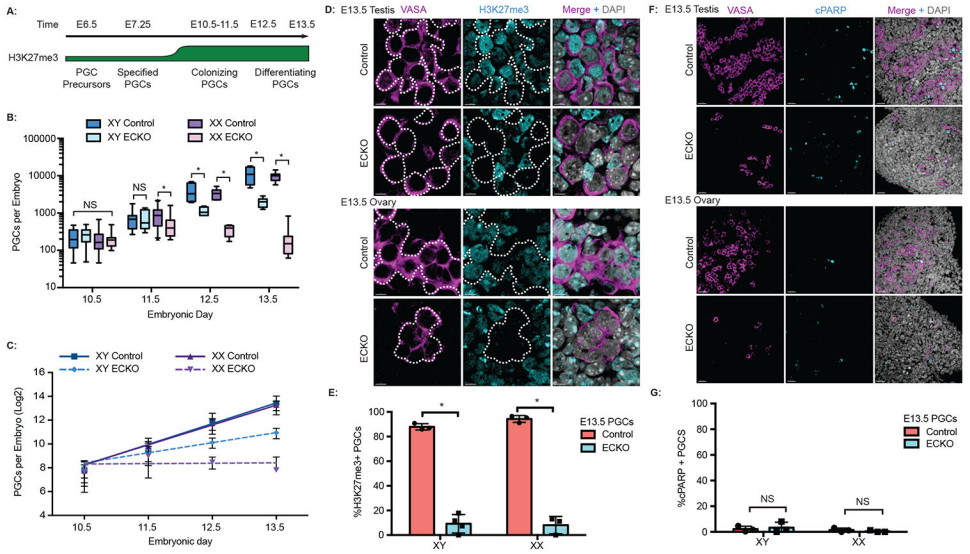

Figure 1:

EED regulates PGC number within the embryonic gonads. A) Schematic of PGC differentiation and the global changes of H3K27me3 in epiblast and PGC nuclei from E6.5- E13.5. B) Quantification of average PGC number at E10.5 (n=15-17 embryos), E11.5 (n=8-24 embryos), E12.5 (n=4-7 embryos) and E13.5 (n=6-8 embryos). C) Linear regression analysis of PGC number in B. D) Representative IF image of H3K27me3 at E13.5 in control and ECKO embryonic gonads. VASA marks PGCs. White dashed lines surround PGCs. Scale bar is 5 μm. E) Ratio of H3K27me3+ PGCs from D. F) Representative IF image of cPARP at E13.5 in control and ECKO embryonic gonads. VASA marks PGCs. Scale bar is 10 μm. G) Ratio of cPARP+ PGCs from F. Significance was calculated using T-test in all panels. * is $p<0.05$. All error bars are ± standard deviation. For all IF, n=3 embryos. See also Figures S1 and S2.

Author Manuscript Author Manuscript Author Manuscript Author Manuscript

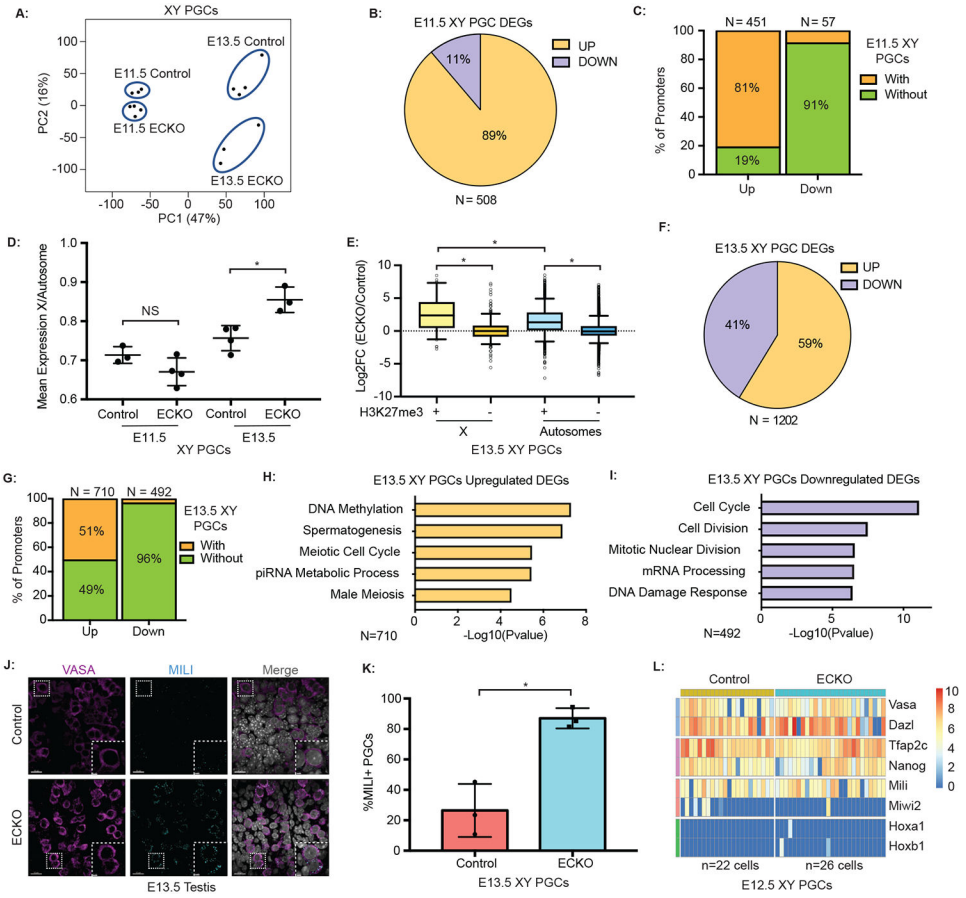

Figure 2:

EED regulates PGC differentiation in the testis. A) PCA plot of RNA-Seq data generated from GFP+ XY PGCs isolated at E11.5 and E13.5. B) Percentage of up and down regulated DEGs at E11.5. C) Percentage of DEGs from B with and without H3K27me3 promoter enrichment in wild-type PGCs at E11.5 (Sachs et al., 2013). D) X-chromosome to autosome expression ratio (X/A) at E11.5 and E13.5. E) Differential log2 fold change in gene expression on the X chromosome and autosomes at E13.5 with (+) and without (−) promoter H3K27me3 enrichment (Liu et al., 2014). F) Percentage of up and down regulated DEGs at E13.5. G) Percentage of DEGs from E with and without promoter H3K27me3 enrichment in wild type PGCs at E13.5 (Liu et al., 2014). H/I) Gene ontology of up (H) and down regulated (I) DEGs at E13.5. Values are calculated based on the −Log10(p-value). DEG number denoted below each plot. J) Representative IF of MILI in control and ECKO embryonic testes at E13.5. VASA marks PGCs. Scale bar is 10 μm. Inset of select nuclei shown in white dashed box with scale bar of 2 μm. K) Ratio of MILI+ PGCs from J. L) Heatmap of selected germ cell marker gene expression from single GFP+ PGCs FACS isolated at E12.5. Blue is germline identity, Purple is early PGC genes, Red is piRNA genes and Green is somatic genes. Color is assigned based on log normalized read counts. Significance was calculated using a T-test. * is $p<0.05$. All error bars are ± standard deviation. For IF, n=3 embryos. See also Figure S3.

Author Manuscript Author Manuscript Author Manuscript Author Manuscript

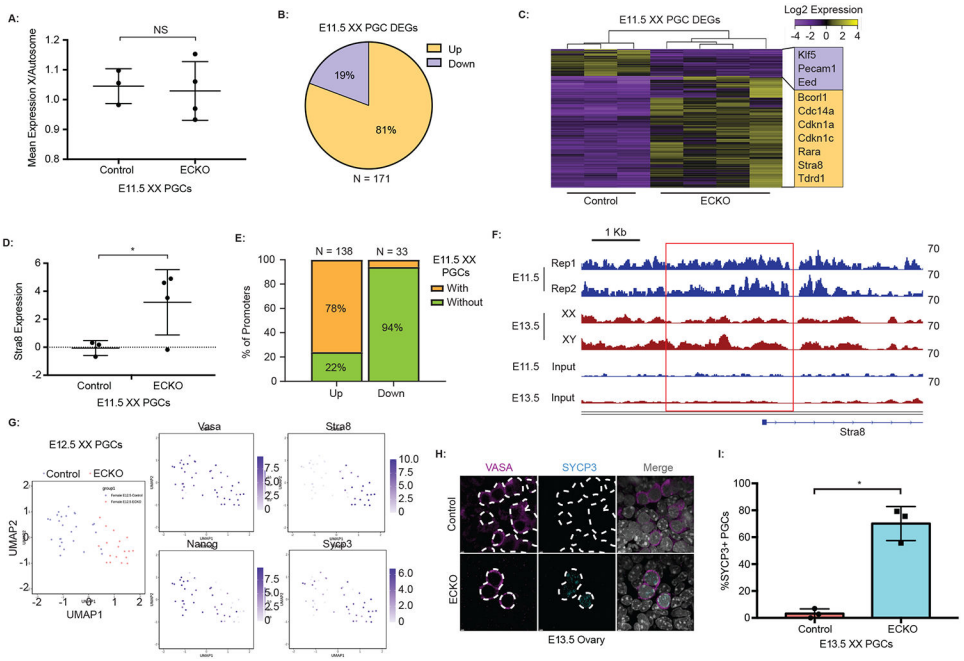

Figure 3:

EED Regulates PGC Differentiation in the Ovary. A) Mean X/A expression ratio in XX PGCs at E11.5. B) Percentage of up and down regulated DEGs at E11.5. C) Heatmap of the 171 DEGs at E11.5. Selected up and downregulated DEGs are displayed. D) *Stra8* Log2 fold change expression of E11.5 control and ECKO PGC replicates. E) Percentage of DEGs at E11.5 with or without promoter H3K27me3 in PGCs (Sachs et al., 2013). F) Genome browser track for H3K27me3 at the *Stra8* promoter at E11.5 (Sachs et al., 2013) and E13.5 (Liu et al., 2014). Promoter region boxed in red (−2 to +0.5 kb). G) UMAP of GFP+ FACS isolated single PGCs analyzed using Smart-seq. Feature plots for the PGC marker *Ddx4* (*Vasa*), the meiotic initiator *Stra8*, the pluripotency marker *Nanog* and the meiotic protein *Sycp3* are highlighted. H) Representative IF of SYCP3 at E13.5. VASA marks PGCs. White dashed lines surround PGCs. Scale bar = 2 μm. n=3 embryos. I) Ratio of SYCP3+ PGCs from H. Significance was calculated using a T-test. * is $p<0.05$. All error bars are ± standard deviation. See also Figures S3 and S4.

Author Manuscript Author Manuscript Author Manuscript Author Manuscript

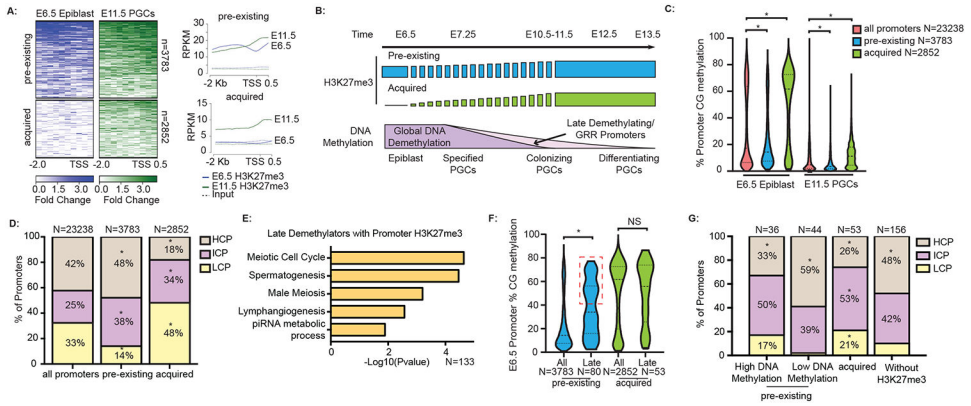

Figure 4:

Gametogenesis genes are co-enriched for H3K27me3 and DNA Methylation in the epiblast. A) Heatmaps of H3K27me3 promoter (−2 to +0.5 kb) enrichment at E6.5 (Yang et al., 2018) and E11.5 (Sachs et al., 2013). Acquired promoters gain H3K27me3 by E11.5 in PGCs compared to E6.5 epiblast. Pre-existing promoters have H3K27me3 in both E6.5 epiblast and E11.5 PGCs. Metaplots for each category are presented. B) Schematic of the gain of promoter H3K27me3 in the pre-existing and acquired subsets with dashed bars showing predicted gains in H3K27me3. The average DNA demethylation of the genome (global) and late demethylating/GRR promoters DNA demethylation are below in purple (Seisenberger et al., 2012). C) %CG methylation (Seisenberger et al., 2012) at E6.5 and E11.5 in promoters defined as either having pre-existing or acquired H3K27me3. Significance within a given time point was calculated via Hypergeometric testing. D) Promoter CpG content analysis of pre-existing or acquired promoters. High, intermediate and low CpG content were defined as described in the methods. E) Gene ontology of the late demethylating promoters with H3K27me3 at E11.5 (Sachs et al., 2013). F) %CG methylation of promoters at E6.5 (Seisenberger et al., 2012) with pre-existing or acquired H3K27me3. Pre-existing promoters with high CG methylation (40%) outlined in red. Significance was calculated using T-Test. G) Promoter CpG content analysis of pre-existing promoters with 40% CG methylation (high) or <40% CG methylation (low) at E6.5 (Seisenberger et al., 2012), acquired promoters and all promoters without H3K27me3 at E6.5 (Yang et al., 2018). * is $p<0.05$. See also Figure S4.

Author Manuscript Author Manuscript Author Manuscript Author Manuscript

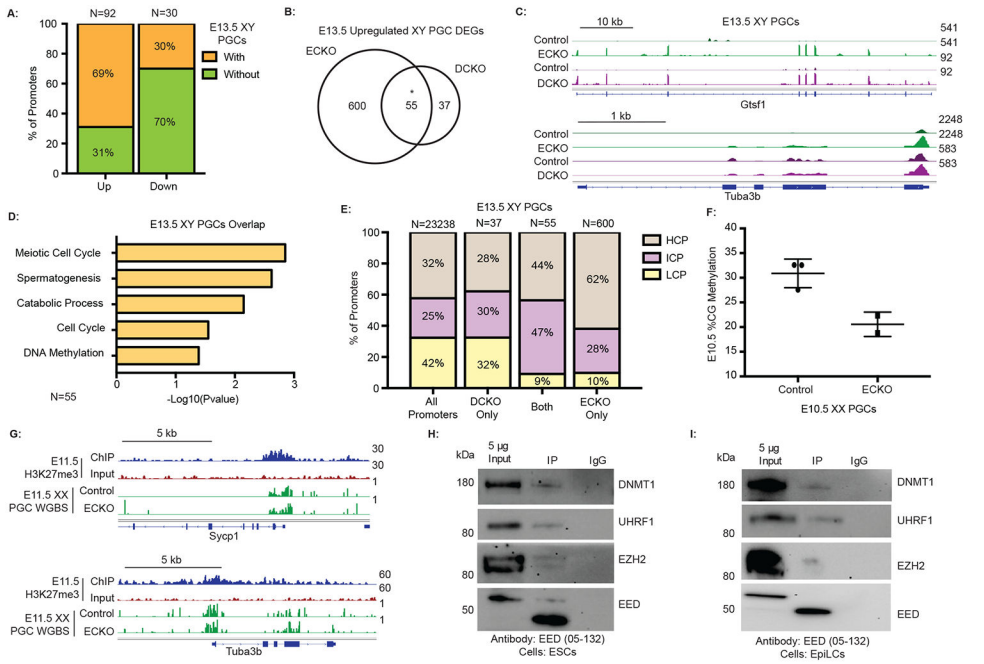

Figure 5:

Gametogenesis genes are co-regulated by EED and DNMT1. A) Percentage of up and down regulated DEGs from E13.5 XY DCKO embryos (Hargan-Calvopina et al., 2016) with and without promoter H3K27me3 (Liu et al., 2014). B) Overlap in upregulated DEGs in XY E13.5 ECKO and DCKO conditions. Significance was calculated via hypergeometric testing. * is $p<0.05$. C) Representative RNA-sequencing tracks from overlapping DEGs in the DCKO (Hargan-Calvopina et al., 2016.) and ECKO data sets D) Gene ontology of the overlapping DEGs in the XY ECKO and DCKO conditions. Values are calculated based on the −Log10(p-value) and DEG number denoted below the plot. E) Promoter CpG content analysis of E13.5 XY ECKO and DCKO overlapping or DCKO only promoters. High, intermediate and low CpG content promoters were defined as described in the methods. F) Percentage of methylated CG sites with 4X coverage in E10.5 XX PGCs as measured by WGBS (n=2 replicates). G) Representative WGBS tracks from E11.5 XX PGCs and E11.5 H3K27me3 ChIP-seq tracks (Liu et al., 2014) at representative overlapping DEGs from ECKO and DCKO embryos (Hargan-Calvopina et al., 2016). H) Representation of co-immunoprecipitation in serum+LIF mouse ESCs following pulldown with an anti-EED antibody (05-132). Input is collected prior to the pulldown, IP is the EED bound fraction and IgG is a negative control reciprocal pulldown with a non-specific mouse antibody (5415) (blots from n=3 independent replicate pull downs for EED (05-132), EZH2 (5246) and DNMT1 (ab87654), n=2 independent replicates for UHRF1 (sc373750)). I) Co-immunoprecipitation in EpiLCs following pulldown with an anti-EED antibody (05-132) (blots from n=3 independent replicates for EED (05-132), DNMT1 (ab87654) UHRF1 (sc373750), n=2 independent replicates for EZH2 (5246)). All replicate and uncropped blots are in Data S1. All antibodies identified by their catalogue number listed in table S3. See also Figure S5.

Author Manuscript Author Manuscript Author Manuscript Author Manuscript

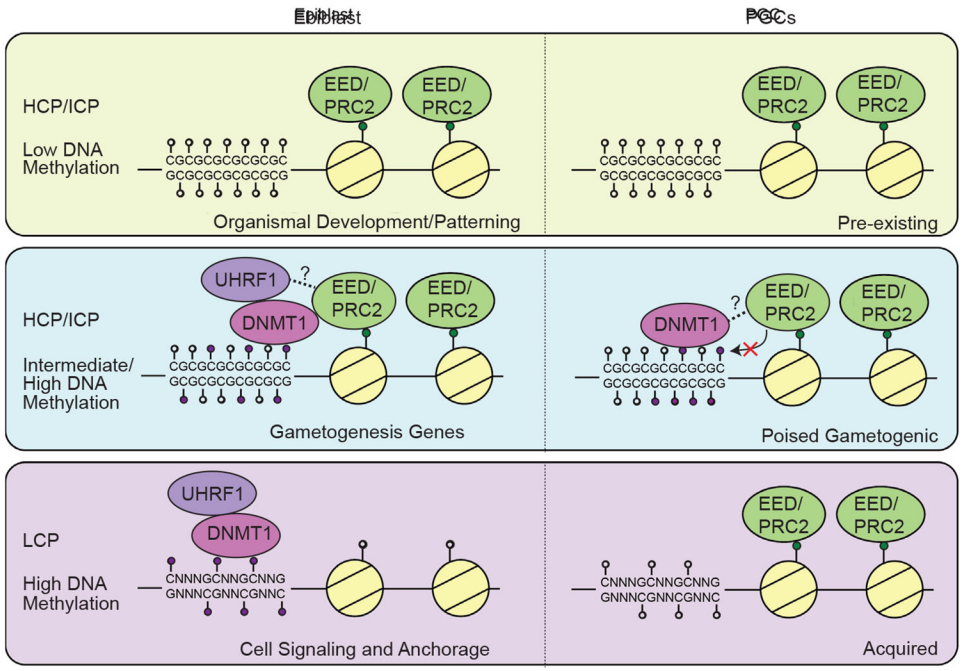

Figure 6:

Model for EED and DNMT1 Co-regulation of Gametogenesis Genes. Promoters that exhibit H3K27me3 in the epiblast and in PGCs (pre-existing H3K27me3) have low levels of DNA methylation. These genes are involved in organismal development. Promoters with detectable H3K27me3 in PGCs but not in the epiblast (acquired H3K27me3) begin with high levels of DNA methylation in the epiblast which reverts to low DNA methylation in PGCs. These genes are involved in cell signaling and anchorage. This study identified a new set of poised gametogenic promoters that begin with H3K27me3 and high levels of DNA methylation in the epiblast. These promoters continue to have detectable H3K27me3 and DNA methylation in PGCs. We propose that the maintenance of this signature in the epiblast is regulated by DNMT1/EED interactions. In PGCs, EED is not required to maintain DNA methylation at gametogenesis genes (red cross). Dotted line in the epiblast represents a potential interaction between UHRF1 in the epiblast as an alternative interacting partner with EED/PRC2. Dotted line between DNMT1 and EED/PRC2 in PGCs represents a theoretical interaction which has yet to be validated.

Author Manuscript Author Manuscript Author Manuscript Author Manuscript

KEY RESOURCES TABLE

REAGENT or RESOURCE	SOURCE	IDENTIFIER
Antibodies		
Antibody details can be found in Table S3	N/A	N/A
Critical Commercial Assays		
Ovation RNA-Seq System V2	NuGen	7102-A01
Ovation Rapid DR Multiplex System 9-16	NuGen	0320-32
Qiagen RNeasy Micro Kit	Qiagen	74004
High Sensitivity D5000 ScreenTape	Agilent Technologies	5067-5592
D1000 ScreenTape	Agilent Technologies	5067-5582
Qiagen MinElute Reaction Cleanup Kit	Qiagen	28206
KAPA Library Quantification Kit Illumina Platforms	Biosystems	KK4824
EZ DNA Methylation Direct kit	Zymo	D5020
Pico Methyl-Seq Library Prep Kit	Zymo	D5455
Smart-seq v4 Ultra Low Input RNA Kit	Takara	634891
Nextera XT DNA Library Prep Kit	Illumina	FC-131-1096
Nextera XT Index Kit v2 Set A	Illumina	FC-131-2001
Nextera XT Index Kit v2 Set D	Illumina	FC-131-2004
Deposited Data		
EED Knockout and Control PGC RNA sequencing	This Paper	GSE139413
E6.5 and E11.5 PGC Whole Genome Bisulfite	Seisenberger et al., 2012	ERP001953
E6.5 Epiblast H3K27me3 ChIP sequencing	Yang et al., 2018	GSE104243
E11.5 PGC H3K27me3 ChIP sequencing	Sachs et al., 2013	GSE46396
E13.5 PGC H3K27me3 ChIP sequencing	Liu et al., 2014	GSE60377
E10.5 and E11.5 Knockout and Control PGC WGBS	This Paper	GSE139413
Nextera XT Index Kit v2 Set D	Illumina	FC-131-2004
Experimental Models: Organisms/Strains		
Mouse: Strain B6;129S1-EED^{tm1sho}	The Jackson Laboratory	RRID:IMSR_JAX:022727
Mouse: Strain B6;129S4-*Pouf5f1*^{tm2Jae}/J	The Jackson Laboratory	RRID:IMSR_JAX:008214
Mouse: Strain B6.Cg-Tg(Prdm1-Cre)1Masu/J	The Jackson Laboratory	RRID:IMSR_JAX:008827
Oligonucleotides		
Genotyping Primers can be found in Table S4	N/A	N/A
Software and Algorithms		
Imaris	Bitplane	RRID: SCR_007370
HTSeq	Anders et al., 2015	RRID: SCR_005514
edgeR	Robinson et al., 2010	RRID: SCR_012802
HISAT2	Kim et al., 2015	RRID: SCR_015530
SAMtools	Li et al., 2009	RRID: SCR_002105
Bowtie2	Langmead and Salzberg, 2012	RRID: SCR_005476

Author Manuscript Author Manuscript Author Manuscript Author Manuscript

REAGENT or RESOURCE	SOURCE	IDENTIFIER
Bedtools	Quinlan and Hall, 2010	RRID:SCR_006646
BS-Seeker 2	Guo et al., 2013	RRID: SCR_005641
Cutadapt 1.18	Martin, 2011	RRID:SCR_011841
Star 2.7.0	Dobin et al., 2013	RRID:SCR_004463
Scater	McCarthy et al., 2017	RRID:SCR_015954
Feature Count 2.0.1	Liao et al., 2014	RRID:SCR_012919
SC3	Kiselev et al., 2017	RRID:SCR_015953
ggPlot2	Wickham, 2016	RRID:SCR_014601
Picard tools	Broad Institute	RRID:SCR_006525
Other		
Covaris Sonicator S2	Covaris	N/A
Illumina HiSeq 4000	Illumina	RRID: SCR_016386
Illumina HiSeq 2500	Illumina	RRID: SCR_016383
NovaSeq 6000	Illumina	RRID: SCR_016387
LSM 880 Microscope	Zeiss	N/A
Agilent 2200 TapeStation	Agilent	RRID: SCR_014994
Mini Gel Tank	Thermo Fisher	N/A
Trans-Blot Turbo Transfer System	BioRad	N/A
ChemiDoc	BioRad	RRID: SCR_021693